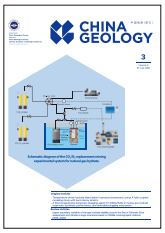
China Geology 9 (2026) 468−488

China Geology

Journal homepage: http://chinageology.cgs.cn
https://www.sciencedirect.com/journal/china-geology



Gas sources of marine gas hydrate systems and the critical role of fluid migration pathways in gas hydrate formation

Jin-xiu Yang[a, b], Chen Wang[a], Ang Li[c, d,*], Yong Zhang[c, d], Li Zhao[a], Kun-yi Liu[a]

[a] *School of Geosciences, China University of Petroleum (East China), Qingdao* 266580, *China*
[b] *Key Laboratory of Deep Oil and Gas, China University of Petroleum (East China), Qingdao* 266580, *China*
[c] *Technology Innovation Center for Marine Methane Monitoring of Ministry of Natural Resources, Qingdao Institute of marine geology, China Geological Survey, Qingdao* 266237, *China*
[d] *Laboratory for Marine Mineral Resources, Laoshan Laboratory, Qingdao* 266237, *China*

ARTICLE INFO

Article history:
Received 6 April 2025
Received in revised form 6 August 2025
Accepted 15 August 2025
Available online 11 October 2025

Keywords:
Gas hydrate
Combustible ice
Clean energy
Free gas zone
Biogenic gas source
Thermogenic gas source
Mixed gas source
Fluid migration pathway
Numerical simulation

ABSTRACT

Gas hydrate systems contain large quantities of methane that may originate from biogenic, thermogenic, or mixed sources. Fluid migration pathways, including gas chimneys, faults, inclined permeable strata and diapirs, are critical for transporting thermogenic gases at depth into gas hydrate systems in shallow subsurface. However, the role of these pathways in hydrate accumulation, particularly in systems dominated by biogenic or mixed gases, remains poorly investigated. This study integrates global case analyses of geochemical indicators of gas origin and geophysical signatures revealing spatial relationships between hydrate systems and migration conduits. Numerical modeling of hydrate accumulation history in the Gulf of Mexico Basin and the Qiongdongnan Basin further has been carried out. Results show that regardless of gas origin, *in-situ* biogenic gas alone is insufficient to form medium- to high-concentration gas hydrate. Fluid migration pathways are necessary for providing allochthonous gas. Generally, this study provides insights into the formation history of gas hydrate system and indicates that fluid migration pathways play a pivotal role in the formation of favorable gas hydrate systems, irrespective of whether the gas source is biogenic, thermogenic, or mixed.

©2026 China Geology Editorial Office.

1. Introduction

The study of gas hydrate is blooming over the past decades due to its potential in energy resources, its feedback from and on climate change and being an uncertain driver for submarine geohazards (Shipley TH et al., 1979; Wiese K and Kvenvolden KA, 1993; Ruppel CD and Kessler JD, 2017). The formation and accumulation of natural gas hydrate are governed by a complex interplay of factors, including temperature and pressure conditions, gas sources, gas migration pathways, and the reservoir properties, which occur on most of the global continental margins (Palodkar AV and Jana AK, 2017). The formation and dissociation of gas hydrate could be caused by the variations of heat flow, sea level, sedimentation, and erosion. Their history over geological time reflects the dynamic shift of the base of gas hydrate stability zone (BHSZ), which is often indicated by a bottom simulating reflection (BSR) on seismic images (Shipley TH et al., 1979).

Fluid migration in hydrate systems involves two primary mechanisms: Diffusion and advection (Leythaeuser D et al., 1982; Berndt C, 2005; Gay A and Berndt C, 2007). Diffusion refers to concentration-driven and relatively slow movement of dissolved gases through pore spaces, which often dominates in low-permeability sediments (Krooss BM et al., 1988; Judd A and Hovland M, 2009). Advection represents the bulk flow of fluids driven by pressure gradients which is often found within fractures or permeable layers, efficiently delivering methane to the hydrate stability zone and affecting its formation and distribution (Kopf AJ, 2002; Gay A et al., 2007). Both mechanisms work together to supply methane, with their relative importance depending on geological conditions such as sediment porosity, fluid pressure, and tectonic activity. Previous studies show that enriched gas hydrate accumulations prefer occurring in advection-dominated systems (Xu WY and Ruppel C, 1999; Haacke RR

First author: *E-mail address*: yangjinxiu@upc.edu.cn (Jin-xiu Yang).
* Corresponding author: *E-mail address*: ang.li_cn@outlook.com (Ang Li).

Literary editor: Xi-jie Chen
doi:10.31035/cg2025061
2096-5192/© 2026 China Geology Editorial Office.

Copyright © 2026 Editorial Office of China Geology. Publishing services by Elsevier B.V. on behalf of KeAi Communications Co. Ltd.
This is an open access article under the CC BY-NC-ND License (http://creativecommons.org/licenses/by-nc-nd/4.0/).

et al., 2007).

The accumulation of gas hydrate and its underlying free gas zone (FGZ) are mainly controlled by methane supply and reserving capacity of sediments (Boswell R et al., 2012; Hillman JIT et al., 2017). Gas origins have been well categorized into three types based on geochemical analysis using hydrate gas $C_1/(C_2+C_3)$ ratios and methane $\delta^{13}C$ values: Thermogenic, biogenic gases and those of mixed origins (Li YY et al., 2022). Thermogenic methane typically exhibits a $C_1/(C_2+C_3)$ ratio <100 and $\delta^{13}C_{VPDB}$ values >−50‰, reflecting its origin from thermal cracking of organic matter. Biogenic methane shows a $C_1/(C_2+C_3)$ ratio >1000 and more depleted $\delta^{13}C_{VPDB}$ values (−55‰–−60‰), indicative of microbial methanogenesis. The values that are between these two endmembers ($100 < C_1/(C_2+C_3)$ ratio <1000 and $-55‰ < \delta^{13}C_{VPDB} < -50‰$) suggest mixed-origin methane, resulting from the combination of both thermogenic and biogenic processes. Recent studies show increasing contribution of thermogenic gases to gas hydrate system (Wang XJ et al., 2014; Zhang ZJ and Wright CS, 2017; Zhang W et al., 2020; Jin JP et al., 2020), and even biogenic gas may be formed by the secondary biodegradation of thermogenic gas which migrated to the shallow sediments where microorganisms consume heavier hydrocarbons and produce microbial methane (Hillman JIT et al., 2017; Li YY et al., 2022). But the proportions of contribution of different gas origins to gas hydrate system has not been well elaborated yet. In addition, seismic imaging of the global gas hydrate systems shows that gas hydrate-containing layers and FGZs often occur at the places where there are fluid pathways such as faults, gas chimneys, diapirs and inclined permeable sand layers (Ren JF et al., 2024; Xia Y et al., 2024). However, the extent to which vertical migration pathways that bypass sedimentary succession contribute to gas hydrate accumulation and affect hydrate composition remains poorly understood.

In this paper, global examples are examined to review the gas origins of hydrate systems and study the role of fluid conduits in the formation of gas hydrate system. Geochemical analyses, geophysical interpretation and numerical simulation methods are used to examine the different combinations of gas sources and evaluate the connection between different gas origins and fluid migration conduits, and their roles in gas hydrate accumulation.

2. Data and methods

2.1. Review of global gas hydrate systems

This study includes 32 worldwide cases, among which 13 have drilling data and 19 have been confirmed to find gas hydrate systems (Fig. 1, Tables 1, 2). The dataset includes 517 well samples from marine gas hydrate systems, including those in Hydrate Ridge, Blake Ridge, and the Gulf of Mexico. Key sample parameters include gas composition (methane C_1, ethane C_2, and propane C_3 percentages) and isotopic values ($\delta^{13}C$ and δD). Hydrocarbon gas isotopic compositions and molar ratios (C_1/C_2 and $C_1/(C_2+C_3)$) are effective indicators for determining natural gas genetic types and origins (Bernard B et al., 1977; Chung HM et al., 1988; Whiticar MJ, 1999; Milkov AV, 2005, 2011; Milkov AV and Etiope G, 2018; Liu QY et al., 2019). Milkov AV and Etiope G (2018) developed a revised genetic diagram correlating $C_1/(C_2+C_3)$ ratios with $\delta^{13}C_1$ values, based on a global dataset of >20000 samples (Fig. 2). This diagram has been widely used to classify natural gas genetic origins, providing a robust framework for

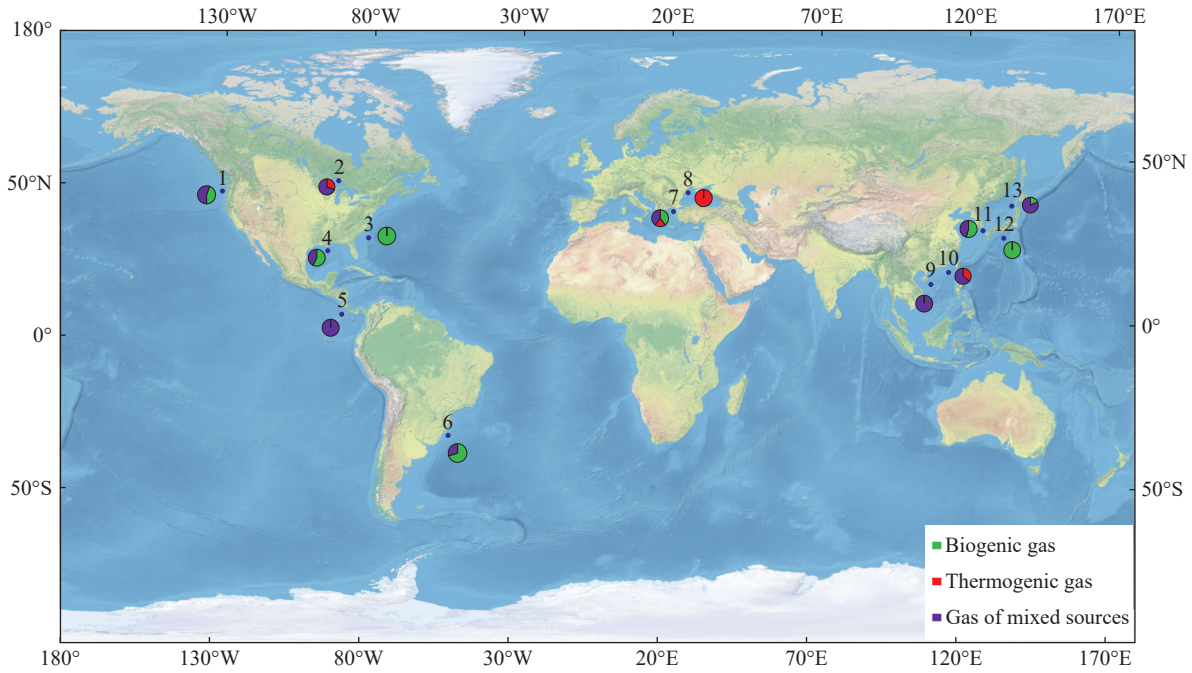


Fig. 1. Global distribution of representative gas hydrate systems and their gas origin types (after Benson TR et al., 2017). 1–Hydrate Ridge, Offshore Oregon/Cascadia Margin; 2–Antrim Shale; 3–Blake Ridge region; 4–Gulf of Mexico; 5–Costa Rica; 6–Rio Grande Cone (Brazil); 7–Sea of Marmara; 8–Homorod seep (Romania); 9–Qiongdongnan Basin; 10–Shenhu; 11–Ulleung Basin; 12–Nankai Trough; 13–Joetsu Basin.

distinguishing biogenic, thermogenic, and mixed-origin gases. It effectively illustrates the gas origins of the case studies investigated in this paper.

Seismic reflection method was used to delineate gas hydrate systems, allowing the identification of BSRs, overlying hydrate-bearing layers, and underlying free gas zones (FGZs). They were also used to interpret fluid migration conduits, deeper hydrocarbon reservoirs, and shallow gas accumulations. Spatial relationships among these units provide insights into the gas origins of hydrate. Specifically, the seismic data from the Gulf of Mexico Green Canyon 955 Well (Haines SS et al., 2017) and Qiongdongnan Basin W08 Well (Lai HF et al., 2021) were analyzed, based on which geological and numerical models are built to predict the fluid migration, hydrate and free gas saturations.

2.2. Numerical modeling

PetroMod software was used to simulate the history of gas hydrate accumulation in this study, and tried to figure out to

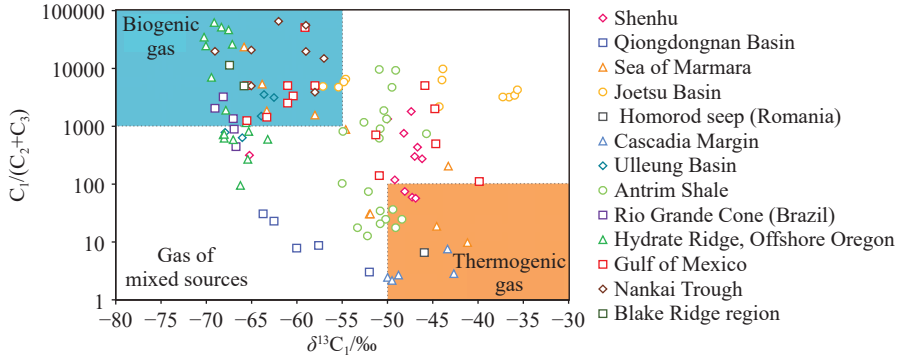


Fig. 2. Genetic types of the hydrate-bound gases reviewed in this study (after Bernard B et al., 1977).

Table 1. Compilation of isotopic and molecular composition data of gases from global gas hydrate systems, with interpreted gas origins.

Location	Well	Depth/m	$\delta^{13}C_{VPDB}$/‰			δD/‰	$C_1/(C_2+C_3)$	Conclusions		Reference
			C_1	C_2	C_3	CH_4				
Shenhu	SC-W01B	135.7	−50	−31	−18.1	−170.3	1338.3	M	M, T	Liang QY et al., 2022
		155.48	−47	−30.5	−18.3	−190.7	302.4	M		
		160.76	−49.2	−28.9	−18.6	−195	119.6	M		
	SC-W01C	147.35	−48.2	−27	−18	−183.5	755.3	M		
		148.21	−47.4	−26.2	−17.6	−186.3	1792.5	M		
		163.46	−48.1	−28.7	−18.3	−191.9	75.4	T		
	SC-W02B	143.54	−46.7	−28.3	−18.2	−185.8	437.3	M		
		144.52	−46.2	−28.6	−18.1	−191.9	276.2	M		
		158.84	−47.3	−28.3	−18	−197.9	60.1	T		
		170.08	−46.9	−27.7	−17.3	−193.5	57.8	T		
	SC-W03B	136.57	−65.2	−43.3	−24.6	−191.3	316.7	M		
	…	…	…	…	…	…	…	…		
Qiongdongnan Basin	4（HY6）	60	−62.5	−28.4	−24.6	/	23.32	M	M	Wei JG et al., 2021
	7（HY20)	63.73	−63.7	−28.8	−23.7	/	31.2	M		
	8(HY9)	63.93	−57.6	−27.9	−24.3	/	8.9	M		
	9	64.53	−60	−29	−25.6	/	8	M		
	12	170.2	−52	−27	−24.4	/	3.1	M		
	…	…	…	…	…	…	…	…		
Sea of Marmara	DV1-PE02	/	−43.3	/	/	−207.4	206	M	M, T, B	Riedel M et al., 2022
	DV2-PE01	/	−44.6	/	/	−220.9	19	T		
	DV3-PE01	/	−52	/	/	−212.3	31	M		
	DV3-PE03	/	−41.2	/	/	−169.7	10	T		
	DV3-PE04	/	−54.6	/	/	−214	880	M		
	DV3-PE06	/	−51.9	/	/	−210.7	31	M		
	DV3-PE09	/	−58	/	/	−214.2	1560	B		
	DV4-PE02	/	−63.8	/	/	−208.1	5285	B		
	DV4-PE08	/	−65.8	/	/	−240.8	23147	B		
	DV5-PE01	/	−63.3	/	/	−252.2	1853	B		
	…	…	…	…	…	…	…	…		

Table 1. (*Continued*)

Location	Well	Depth/m	$\delta^{13}C_{VPDB}$/‰			δD/‰	$C_1/(C_2+C_3)$	Conclusions		Reference
			C_1	C_2	C_3	CH_4				
Joetsu Basin	MD179-3305G	/	−36.6	−17.9	5.8	−167	3158	M	M, B	Hachikubo A et al., 2015
		/	−36	−18.2	5.7	−164	3389	M		
	MD179-3306	4.5[mbsf]	−37.3	−18.4	6.3	−164	3176	M		
		/	−35.7	−18.1	4.8	−167	4213	M		
		/	−54.6	−31.8	/	−195	6446	M		
		/	−54.8	−31.9	/	−194	5758	B		
		/	−57.1	−31.4	−5.3	−194	4819	B		
		/	−55.4	/	/	−195	4713	B		
	MD179-3318C	1.5[mbsf]	−44	−21.3	4	−189	6257	M		
		/	−44.3	−24.5	/	−190	2172	M		
		/	−43.9	−21.4	/	n.d.	9682	M		
	…	…	…	…	…	…	…	…		
Homorod seep (Romania)	H10_seep 4f (9/09)	/	−45.96	−33.04	/	−110	6.7	T	T	Etiope G et al., 2011
	Praid seep(6/07)d	/	−29	nd	/	−193.6	293.9	T		
	…	…	…	…	…	…	…	…		
Cascadia Margin	R694	/	−43.4	−25.5	−23.5	−143	7.74	T	T	Pohlman JW et al., 2005
	R695	/	−42.7	−25.7	−23.6	−140	2.92	T		
	4215	/	−50	−28.8	−25.4	−153	2.51	T		
	4216	/	−48.8	−28.5	−25.8	−179	2.76	T		
	4220	/	−49.5	−28.7	−25.7	−192	2.22	T		
	…	…	…	…	…	…	…	…		
Ulleung Basin	UBGH2-7	6.5	−63.9	/	/	−197	1489	B	M, B	Riedel M et al., 2022
		24.7	−67.9	/	/	−194	782	M		
	UBGH2-7	35.4	−66	/	/	−190	636	M		
	UBGH2-11	53.4	−62.5	/	/	−201	3127	B		
		99.5	−63.6	/	/	−198	3526	B		
	…	…	…	…	…	…	…	…		
Antrim Shale	6	/	−50.8	/	/	−238	906	M	M, T	Martini AM et al., 1998
	7	/	−45.7	/	/	−236	742	M		
	8	/	−54.9	/	/	/	810	M		
	10	/	−55	/	/	/	104	M		
	22	/	−49.4	/	/	−217	37	T		
	39	/	−50.8	/	/	−220	35	M		
	44	/	−52.1	/	/	−246	75	M		
	51	/	−50.2	/	/	−209	25	M		
	57	/	−52.6	/	/	−258	1168	M		
	73	/	−49.5	/	/	−255	4679	M		
	74	/	−50.9	/	/	/	9435	M		
	87	/	−53.3	/	/	/	18	M		
	91	/	−48.4	/	/	−227	25	T		
	94	/	−49.1	/	/	−225	18	T		
	116	/	−50.4	/	/	−235	1866	M		
	147	/	−50.9	/	/	−232	623	M		
	150	/	−50.8	/	/	−260	21	M		
	153	/	−50.1	/	/	−237	1332	M		
	160	/	−49.1	/	/	−227	9159	M		
	169	/	−52.2	/	/	−222	13	M		
	…	…	…	…	…	…	…	…		
Rio Grande Cone (Brazil)	PC76	727.5	−68.1	/	/	/	3210	B	M, B	Miller DJ et al., 2015
	PC76	892	−69	/	/	/	2040	B		
	PC67	508.5	−67	/	/	/	1352	B		
		853	−66.9	/	/	/	890	M		
		988	−66.7	/	/	/	446	M		
	…	…	…	…	…	…	…	…		

Table 1. (*Continued*)

Location	Well	Depth/m	$\delta^{13}C_{VPDB}$/‰			δD/‰	$C_1/(C_2+C_3)$	Conclusions		Reference
			C_1	C_2	C_3	CH_4				
Hydrate Ridge, Offshore Oregon	1244	65	−67.1	−43.2	/	/	25663	B	M, B	Milkov AV et al., 2005
		74.2	−68.3		/	−208	50583	B		
	1245	54.53	−69.1	−45.3	/	−203	60730	B		
		85	−67.5	−46.7	/	−188	45431	B		
	1247	93.01	−70	−52.5	/	−202	24150	B		
	1248	0.5	−68.1	−36.9	−25.6	−202	713	M		
		7.37	−66.2	−30.9	−26.6	/	96	M		
		87	−67.8	−42.1	/	−204	1881	B		
	1249	1.95	−65.3	/	/	/	813	M		
		6.06	−67	−34.6	−23.1	−200	588	M		
		19.6	−65.4	−33.5	−23.1		269	M		
		2.11	−68	/	/	/	620	M		
		0	−68	−33.7	−22	/	725	M		
		16.14	−63.2	/	/	−198	597	M		
	1250	1.64	−65.6	−31.1	/	−193	1148	B		
		81.53	−69.4	−49.3	/	−200	6935	B		
		100.23	−70.2	−48.3	/	−202	33981	B		
	…	…	…	…	…	…	…	…		
Gulf of Mexico		40	−61	/	/	/	4999	B	M, B	Bernard BB et al., 1976
		50	−58	/	/	/	4999	B		
		30	−51.3	/	/	/	710	M		
		57	−50.9	/	/	/	142	M	M, B	
		44	−65.5	/	/	/	1249	B		
		55	−44.7	/	/	/	498	M		
		81	−45.9	/	/	/	4999	M		
		75	−44.8	/	/	/	1999	M		
		70	−61	/	/	/	2499	B		
	…	…	…	…	…	…	…	…		
Nankai Trough	AT1-C-8P(190-198)	279.94	−62	/	/	/	63758	B	B	Kida M et al., 2015
	AT1-C-10P(33-93)	284.63	−65	/	/	/	20535	B		
	AT1-C-10P(177-187)	285.82	−69	/	/	/	19459	B		
	AT1-C-14P(26.5-36.5)	296.315	−59	/	/	/	54581	B		
	AT1-C-18P(153-186)	309.695	−59	/	/	/	19274	B		
	AT1-C-18P(198.5-231)	310.148	−57	/	/	/	14693	B		
	AT1-C-20P(120-136)	315.28	−58	/	/	/	3863	B		
	AT1-C-20P(136-145)	315.405	−65	/	/	/	4933	B		
	…	…	…	…	…	…	…	…		
Blake Ridge region	994	259.9	−67.4	/	/	−205	11225	B	B	Borowski WS, 2004
	997	331	−65.8	/	/	−196	4926	B		
	…	…	…	…	…	…	…	…		
Costa Rica	GH01		−43.3	/	/	−125	3069	M	M	Schmidt M et al., 2005
	GH02		−45.2	/	/	−135	2150	M		
	GH03		−43.4	/	/	−143	3029	M		
	GH04		−44.6	/	/	−143	2972	M		
	…	…	…	…	…	…	…	…		

Notes: T–Thermogenic; B–biogenic; M–mixed source.

what degree the migration pathways play a role in this accumulation. The workflow of PetroMod simulation involves integration of geological, geochemical, and geophysical data that are used to constrain the behavior of hydrocarbon generation and the properties of rocks and fluid units. The process begins with the setting up of a geological model, which includes stratigraphic layers, fault systems, and fluid migration pathways such as gas chimneys, fractures, and permeable strata. Physical parameters of ambient conditions, including temperature, pressure, salinity, and geothermal gradient, are input to determine the depth of the BHSZ. The consistence of modeled BHSZ with the observation of BSR may suggest the rationality of the input parameters. The migration of free gas methane through porous media and fractures is simulated using the embedded simulation method of Darcy's law (Eq. 1):

Table 2. Characteristics of migration channels related to natural gas hydrate system.

Location	BSR depth/(TWT/s)	Hydrate system	Correlation channel	GHL Location	References
Offshore Mauritania	0.88–3.0	BSR, GHL, FGZ	Fault, Diapir	Above the BSR	Yang JX et al., 2013
Qiongdongnan Basin	2–2.5	BSR	Mud diapir, Gas chimney	/	Liang JQ et al., 2019
Active Margins off SW Taiwan	2.0–2.4	BSR, GHL, FGZ	Gas chimney, Permeable sand layer	Above the BSR	Lin LF et al., 2022
Lw3 Area: The Northern Slope of the South China Sea	1.9–2.0	BSR, GHL, FGZ	Fault	Above the BSR	Yan CZ et al., 2020
Krishna-Godavari Basin	2.75–3.13	BSR, GHL, FGZ	Permeable sand layer	Within the GHSZ and high above the BSR	Satyavani N et al., 2015
Shenhu drilling area in South China Sea	1.9–2.1	BSR, FGZ	Mud diapir, Gas chimney, Permeable sand layer	/	Fu C et al., 2019; Zhong SL et al., 2021
Porangahau Ridge	3.4–3.6	BSR, GHL, FGZ	Permeable sand layer	Within the GHSZ and high above the BSR	Schwalenberg K et al., 2010
Offshore Colombia	1.5–2.5	BSR	Fault, Permeable sand layer	/	Rincón-Martínez D et al., 2022
Eastern South Korea Plateau (ESKP), East Sea (Japan Sea)	1.0–1.4	BSR, GHL, FGZ	Gas chimney, Permeable sand layer	Above the BSR	Horozal S et al., 2017
Fiordland margin SW	1.2–2.9	BSR, GHL	/	Above the BSR	Crutchley GJ et al., 2007
Northern deepwater Gulf of Mexico	1.74–2.43	BSR, GHL, FGZ	Fault, Permeable sand layer	Above the BSR	Dai JC et al., 2004

$$v_g = -\frac{k}{\mu_g}\nabla P \tag{1}$$

where v_g is gas velocity, k is permeability, μ_g is gas viscosity, and ∇P is the pressure gradient. This step ensures that the gas migration pathways are accurately represented, including the role of faults, diapirs, and inclined strata in transporting methane to the gas hydrate stability zone (GHSZ).

The core of the simulation involves modeling the dynamic processes of gas hydrate formation and accumulation. PetroMod solves coupled equations for fluid flow, heat transfer, and chemical reactions. The mass balance equation (Eq. 2) for methane gas is expressed as:

$$\frac{\partial\left(\phi\rho_g S_g\right)}{\partial t} + \nabla\cdot\left(\rho_g v_g\right) = Q_g \tag{2}$$

where ϕ is porosity, ρ_g is gas density, S_g is gas saturation, v_g is gas velocity, and Q_g represents the source or sink of methane gas. This equation ensures that the gas supply and accumulation are dynamically simulated over time.

The phase transition from free gas to gas hydrate is governed by kinetic and thermodynamic constraints. The rate of hydrate formation is modeled using a kinetic equation (Eq. 3):

$$\frac{\mathrm{d}S_h}{\mathrm{d}t} = k_h\left(S_g - S_{eq}\right) \tag{3}$$

where S_h is hydrate saturation, k_h is the kinetic rate constant, S_g is gas saturation, and S_{eq} is the equilibrium gas saturation for hydrate formation. This equation captures the time-dependent nature of hydrate formation and its dependence on gas availability and thermodynamic stability. The simulation outputs include hydrate saturation distribution, FGZ characteristics, and fluid migration pathways. By integrating seismic data, well logs, and geochemical analyses, PetroMod provides the details of the history of gas hydrate accumulation processes. The equations used to constrain the lithologies in the model are shown in Table 3 (Manger GE, 1963).

Two cases, including the Gulf of Mexico and Qiongdongnan Basin, are selected and modeled to show the roles of different configurations of methane origin (biogenic and mixture), migration pathway and lithology in controlling the accumulating of gas hydrate. The gas hydrate system in the Gulf of Mexico mainly has the biogenic gas origin (Frye M et al., 2008) and the stratigraphy is characterized by inclined strata due to the well-developed fold belt (Haines SS et al., 2017). The gas hydrate system in the Qiongdongnan Basin has the mixed gas origin, where the structures of basement uplift and accompanied faults occur (Lai HF et al., 2021; Zuo TN et al., 2022). Modeling of the two cases can reveal the controls of different gas origins and structural features on the spatial distribution of hydrates and underlying free gas, which help predict favorable locations of high saturation gas hydrate systems. The parameters of physical properties used in the heterogeneous geological model to constrain the lithologies are shown in Table 4.

3. Geochemical analysis of gas origins

Hydrate-bound gases originate from three primary origins including biogenic, thermogenic and mixed (Collett TS et al., 2019). In marine sediments, biogenic gas forms through anaerobic degradation of organic matters such as ancient biological remnants and plant residues (Brocławik O et al., 2020). It primarily comprises hydrocarbon gases (e.g., methane, ethane) with minor hydrogen sulfide, carbon dioxide, and other constituents (Schoell M et al., 1983). Thermogenic gas forms through thermal cracking of organic and/or inorganic matter at deep depth under high temperature and pressure conditions. These gases, which include

Table 3. Equations used to constrain the lithologies in the model.

Parameters	Equations
Porosity (ϕ) of sand-rich sediments	$\phi = 0.435 - 0.0294\sigma_{eff}^{0.146}$
Porosity (ϕ) of mud-rich sediments	$\phi = (3.9668 - \log(\sigma_{eff}))/10.3618$
Permeability (k_s) of sand-rich sediments	$k_s = 10^{11.20\phi - 18.30}$
Permeability (k_s) of mud-rich sediments	$k_s = 10^{7.97\phi - 21.2}$
Capillary pressure (P_{c_s}) of sand-rich sediments	$P_{c_s} = -0.1\phi + 0.059$
Capillary pressure (P_{c_s}) of mud-rich sediments	$P_{c_s} = -0.5\phi + 2.975$

Notes: σ_{eff} is vertical effective stress in MPa. k_s is the rock permeability without hydrate enrichment in m^2. P_{c_s} is the capillary pressure of rock without hydrate enrichment in MPa.

Table 4. Rock physical parameters in heterogeneous geological model.

	Silt	Mudstone	Chimney structure
Lithologic	75% sands, 25% silt	50% shale, 50% silt	50% shale, 50% silt
Critical saturation of gas migration	0%	0%	0%
Gas saturation required to form hydrates	0.2%	5%	100%
Porosity	$0.435 - 0.0294\sigma_{eff}^{0.146}$	$(3.9669 - \log(\sigma_{eff}))/10.3618$	$(3.9669 - \log(\sigma_{eff}))/10.3618$
Permeability, m^2	$10^{11.20\phi - 18.30}$	$10^{7.97\phi - 21.20}$	$10^{7.97\phi - 19.20}$
Capillary pressure, MPa	$-0.1\phi + 0.0590$	$-0.5\phi + 2.975$	$-0.0253\phi + 0.1502$
Organic carbon content	0%	1%	0%
Hydrogen exponent	0	300mgHC/gTOC	0
Capillary pressure of pure hydrate layer, MPa	0.2	0.2	0.2
Permeability of pure hydrate layer, m^2	10^{-17}	10^{-17}	10^{-17}

hydrocarbons and rare gases such as carbon monoxide and helium, are formed through chemical reactions and geothermal processes occurring within deep geological structures (Sherwood OA et al., 2013).

Natural gas hydrate often contains mixed-origin gases, which formed through the combination of diverse origins, primarily the coexistence of biogenic and thermogenic gases. The presence of mixed-origin gases indicates the mixture of multiple gas types within the hydrate systems (Fu SY and Lu JA, 2010; Wu NY et al., 2011; Liu CL et al., 2015; Dai JX et al., 2017), indicating the complexity of gas origin processes. According to the modeling result by Sun LY et al. (2020), about 80% of the methane-forming hydrate have the thermogenic origin at sites W19 and W17, indicating the more contribution of thermogenic gases than biogenic ones there.

Early studies suggested the dominance of biogenic origins for hydrate-bound gases. Afterwards, increasing number of thermogenic gases have been found in gas hydrate system (Li YY et al., 2022). Recent studies show that thermogenic gases play an increasingly important role in the accumulation of gas hydrate (Fig. 3; Wang XJ et al., 2014; Zhang ZJ and Wright CS, 2017; Jin JP et al., 2020; Zhang W et al., 2020). In this study, gas origin types of gas hydrate are examined based on 13 study areas with confirmed natural gas hydrate occurrences (Table 1). Mixed-origin gas predominated (55% of total gas samples), followed by biogenic (32%) and thermogenic (13%) gases. This indicates that natural gas hydrate gases may derive from multiple sources rather than one single one. For example, thermogenic gases may have been transported to shallow sediments through migration pathways, such as faults and gas chimneys, where they intermingled with biogenic gas forming the gas hydrate system. However, geochemical analysis alone sometimes fail to determine the specific gas source and migration routes. It is also necessary to carry out geophysical interpretation of the gas hydrate system and related fluid migration pathways, as well as numerical modeling of gas hydrate accumulation. Based on all these investigations together, the gas hydrate accumulation processes and their major controlling factors can be better understood.

4. Geophysical evidence of gas hydrate systems and gas migration pathways

4.1. Gas hydrate systems

The presence of gas hydrate significantly influences the propagation velocity of seismic waves (Ojha M and Sain K, 2009). BSR is a reliable seismic indicator of gas hydrate presence and a response to the theoretical base boundary of the GHSZ (Rodrigo C et al., 2009). It is typically parallel to the seafloor or intersecting sediment reflections near the seafloor, and often featured by high reflection amplitude and negative polarity which indicate a marked decrease in acoustic impedance, marking the transition from hydrate-bearing sediments to underlying free gas (Shipley TH et al., 1979; Schwalenberg K et al., 2010). Seismic reflection imaging and full-waveform inversion are essential for acquiring high-resolution stratigraphic images, significantly improving the precision of locating hydrate reservoir (Priest JA et al., 2009).

The integration of well-logging data and seismic prediction techniques is very useful in estimating the

parameters of gas hydrate layers and underlying free gases, including extent, thickness, and saturation. Well-logging data, particularly resistivity and acoustic logs, provide measurements of hydrate saturation and thickness, while seismic attributes, such as amplitude versus offset (AVO) analysis, enhance the spatial mapping of these parameters (Lee MW and Collett TS, 2009; Collett TS et al., 2019). Studies have shown that gas hydrate saturation typically ranges from 10% to 40% within the GHSZ, and higher-saturation ones are often near the BHSZ (Boswell R et al., 2012). The underlying free gas layer, characterized by low seismic velocities and high attenuation, usually exhibits saturations below 10% and is confined to a thin zone immediately below the BSR (Hornbach MJ et al., 2004). For example, the water depth of the W17 Well in the Shenhu area of the South China Sea is approximately 1252 m, and the drilling depth is about 300 m below the seabed (Fig. 4a). The thickness of the hydrate layer is ca. 43.1 m, with an average saturation of ca. 19.4%. There is free gas under the natural gas hydrate layer. The thickness of the free gas layer is ca. 12.0 m, with an average saturation of ca. 30.1%. The water depth of W18 Well is ca. 1282 m, with a drilling depth of ca. 250 m below the seabed (Fig. 4b). The thickness of the natural gas hydrate layer is ca. 11.6 m, while the thickness of the free gas

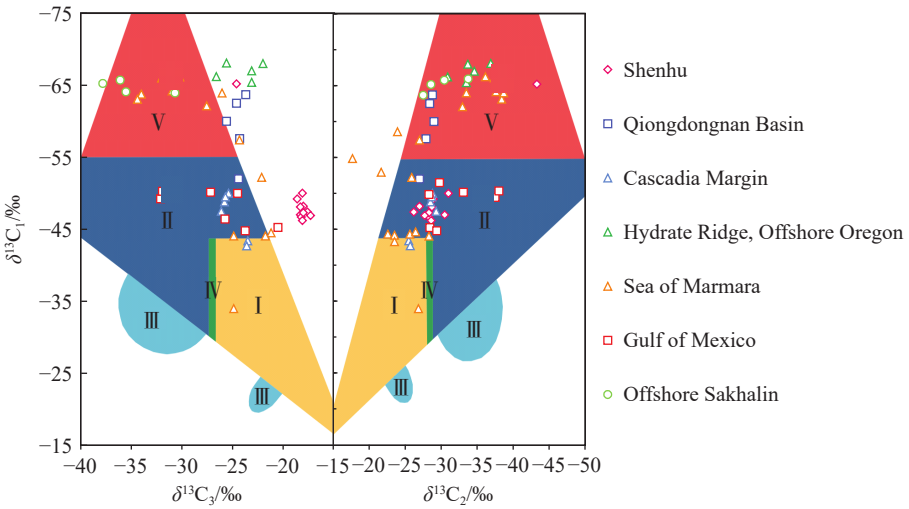


Fig. 3. $\delta^{13}C_1$, $\delta^{13}C_2$, and $\delta^{13}C_3$ values of the hydrate-bound gas samples (after Dai JX et al., 2008). I–Humic type gas; II–sapropel type gas; III–gas mixture with the reversal of carbon isotope; IV–humic type gas and sapropel type gas; V– biogenic gas.

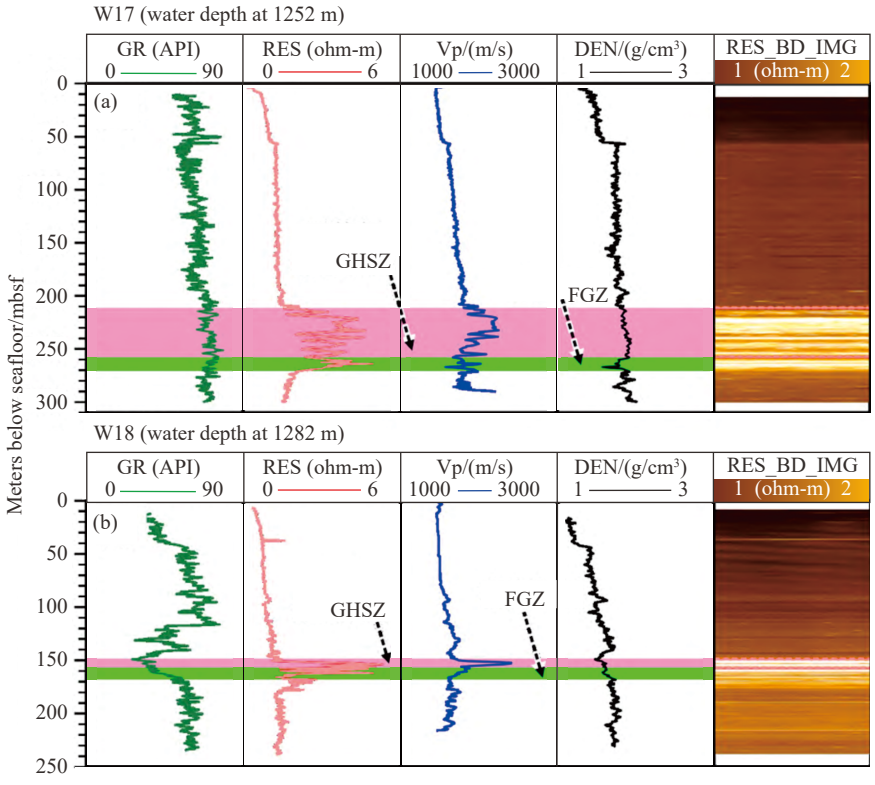


Fig. 4. Logging results at W17 and W18 drilling sites in Shenhu area (after Ren JF et al., 2023).

layer is ca. 28.9 m. The average saturation of the hydrate layer is ca. 30.5% (Ren JF et al., 2023). Generally, the gas hydrate layer predominantly resides within a specific region above the BSR, with its distribution and saturation influenced by local geological and thermal conditions (Sain K and Gupta H, 2012). This integrated approach not only refines reservoir characterization but also aids in assessing the resource potential and stability of gas hydrate systems.

4.2. Gas migration pathways

Methane required for gas hydrate formation could migrate through thin or thick sedimentary succession (Fig. 5; Milkov AV, 2005; Pohlman JW et al., 2009; Riedel M et al., 2010; Collett TS et al., 2010). Extensive laboratory and field studies have identified multiple gas migration pathways associated with diverse geological features which provide methane source for gas hydrate systems, such as gas chimneys (Hutchinson DR et al., 2009; Wang X et al., 2011; Sun QL et al., 2012, 2017; Chen DX et al., 2013; Choi JY et al., 2013; Su M et al., 2014, 2016, 2017), fault systems (Inks TL et al., 2009), fluid diapirs (Xie XN et al., 1999; Wang ZF et al., 2004; Lei C et al., 2011), mud diapirs (Behrens EW, 1984; Van Rensbergen P et al., 1999; Wang FZ and Huang JB, 2008; Hsu HH et al., 2017), magma diapirs and igneous bodies (Cartwright J et al., 2007; Schofield N and Jolley DW, 2013; Sun QL et al., 2014), salt diapirs (Trusheim F, 1960; Haines SS et al., 2017), and inclined/dipping permeable sand layers with comparatively high porosity and permeability, which enable lateral and updip transport of gas-charged fluids under buoyancy and pressure gradients (Boswell R et al., 2012; Davies RJ et al., 2024).

Hydrofracturing within the impermeable sediments may cause the formation of gas chimneys, and result in their higher permeability and porosity than surrounding sediments (Cartwright J et al., 2007; Han WC et al., 2021). Gas chimneys can transport fluids upwards and sustain the formation of gas hydrate through complex networks of small fractures (Yang R et al., 2015; Su M et al., 2016, 2017). On seismic profiles, they are often identified by low amplitude, low frequency and low coherence, appearing as chaotic or diffuse features probably due to the upward fluid migration along gas chimney structures (Coren F et al., 2001; Yang R, 2015). The high reflectivity zone observed at gas chimney apices is interpreted to be caused by free gas accumulation (Chen DX, 2013; Wang XJ et al., 2014; Yang R et al., 2015; Qian J et al., 2018). In some cases, the uppermost ends of gas chimneys may reach the seafloor, forming seafloor expressions such as pockmarks. These seafloor expressions are commonly interpreted as indicators of fluid seepage and represent significant geomorphological markers of subsurface fluid migration processes. For example, many gas chimneys occur above the chaotic mass transport deposit (MTD) in the Ulleung Basin (Bahk JJ et al., 2009; Horozal S et al., 2009; Haacke RR et al., 2009), which originate below the BSR and terminate at various stratigraphic depths (Fig. 6). Some can reach widths of up to 2 km and extend to the seafloor (Horozal S et al., 2009; Kim JH et al., 2011, 2013). Based on seismic data and gas chemistry analysis of piston core samples (depth <8 m), Kim JH et al. (2012) documented upward migration of deep biogas through chimneys in the basin, leading to significant gas hydrate formation in shallow sediments.

In most of gas hydrate provinces, faults act as the predominant fluid migration pathways, and can be readily identified by aligned reflection offsets on seismic profiles (Xie HY et al., 2016). Faults can connect deep strata to the shallow gas hydrate system, and the high-amplitude anomalies (HAAs) indicating hydrate or free gas presence often exist at fault tops. This strong spatial relationship suggests that faults play a crucial role in providing gas for the formation of both gas hydrate and underlying free gas zone. Specifically, an assessment of the isotopic and hydrocarbon composition of hydrate-bound gas and those collected from the emission sites of Buckley Canyon at the Cascadia margin revealed that the hydrate methane has $\delta^{13}C_{VPDB}$ value ranging from −50‰ to −42‰ and δD_{VPDB} value ranging from −143‰ to −138‰ (Pohlman JW et al., 2005). This isotopic signature indicates thermogenic origin of gas for the hydrate in this area. Considering the spatial relationship between the faults and high-amplitude gas hydrate systems (Riedel M et al., 2022), the authors propose that faults play a key role in transporting thermogenic gas from deep to shallow gas hydrate systems (Fig. 7).

Diapirs typically develop under compressional tectonic stress (Lei C et al., 2011). They are caused by the upward movement of mud, salt or igneous intrusions, which create domal structures that disrupt the overlying sediments and thus cause the formation of radial fault systems and fracture networks (Stewart SA, 2006; Sarhan MA, 2023). Differential compaction around the flanks of diapirs generates localized stress fields that promote fracture and fault development in overlying and adjacent strata (Maillard A et al., 2003). The diapir-associated fault and its surrounding fracture networks act as preferential fluid migration pathways, allowing for focused fluid flow (e.g., thermogenic gas) toward the shallow GHSZ (Sarhan MA, 2023). Diapiric structures are typically identified by the domal units of acoustic turbidity or chaotic reflections on lowermost part of seismic profiles (Chen SC et al., 2014). Moreover, the tops of diapir structures often co-exist with associated faults and gas chimneys, together facilitating the upward migration of deep thermogenic gas. When fluids reach the GHSZ, they contribute to the formation of gas hydrate system (Table 2).

Generally, seismic interpretation can reveal the distribution of the gas hydrate systems and fluid migration pathways, as well as their spatial relationship. To better understand the history of gas hydrate accumulation, numerical simulations are essential for precisely delineating fluid migration pathways and reconstructing the dynamic accumulation history.

5. Numerical modeling of gas hydrate accumulation

Numerical simulation methods are essential for studying natural gas hydrate accumulation, which enable quantitative calculations of formation temperatures, hydrocarbon generation capacity, gas hydrate stability zone thickness, fluid migration modes/directions and hydrate saturation. This approach reveals how gas origin conditions and migration pathways influence the accumulation of hydrates and underlying free gas. In this paper, two 2-D models were built based on representative seismic profiles and reservoir heterogeneity in Gulf of Mexico's Green Canyon and South China Sea's Qiongdongnan Basin, to describe the controls of lithologies and fluid migration conduits on biogenic and

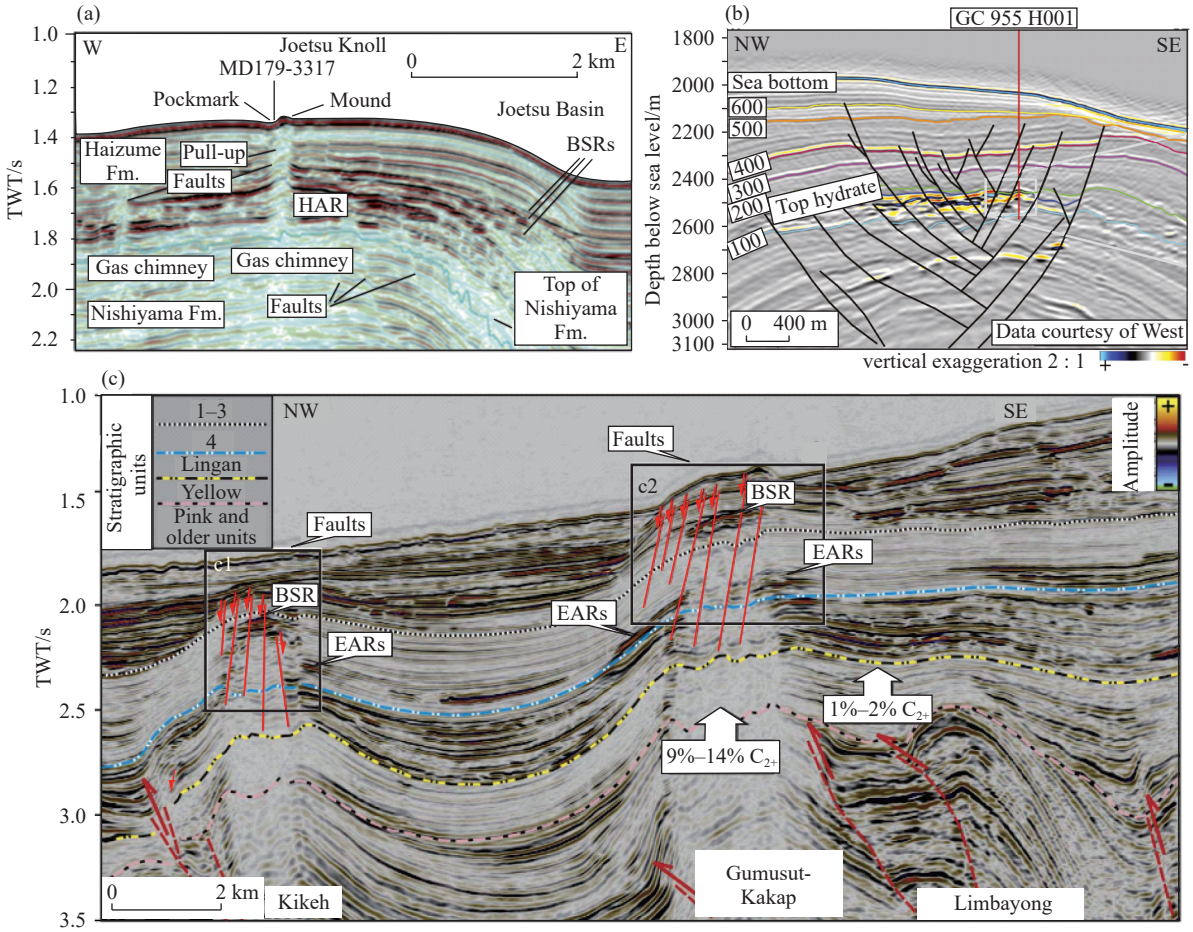


Fig. 5. Seismic profiles showing gas migration pathways. a–Gas chimney on the Joetsu Knoll, eastern margin of the Sea of Japan (Nakajima T et al., 2014); b–faults at Green Canyon 955, Gulf of Mexico (Haines SS et al., 2017); c–normal faults (red solid line) and thrust faults (red dotted line) in the fold and thrust belt offshore Sabah (Paganoni M et al., 2018). HAR–High amplitude reflection; EARs-enhanced amplitude reflections.

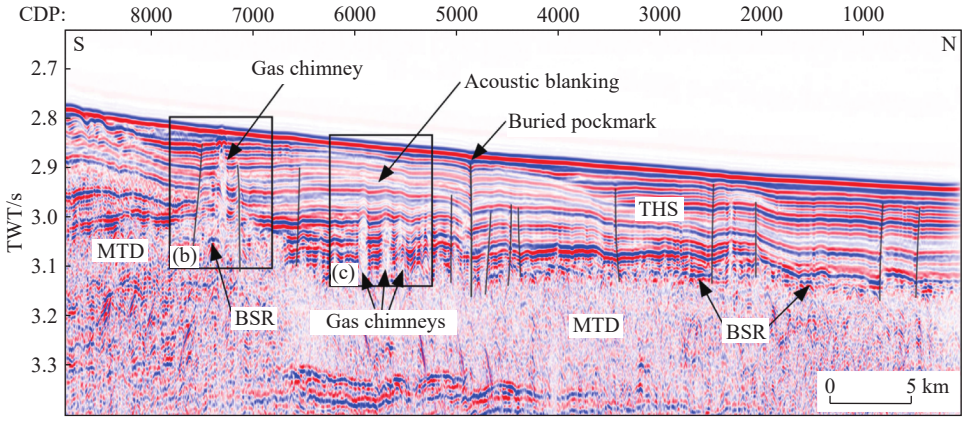


Fig. 6. Seismic profile of the Ulleung Basin showing the distribution of gas chimneys above the MTD (after Yoo DG et al., 2013). The CDP (common depth point) spacing is 6.25 m. MTD—Mass-transport deposits; THS—turbidite-hemipelagic sediments; BSR—bottom simulating reflector.

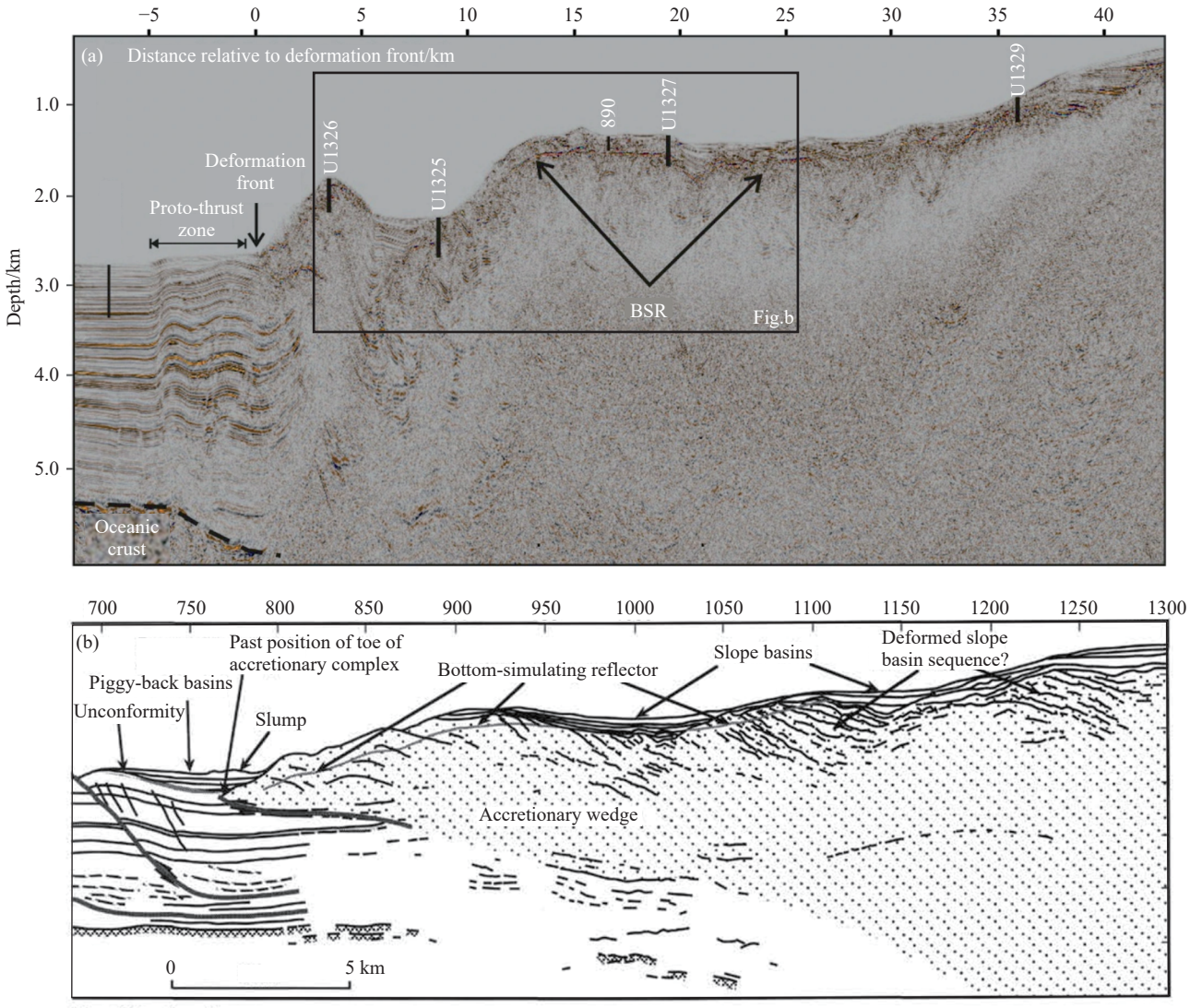


Fig. 7. a–Seismic profile of the Cascadia Basin showing the distribution of the BSR (after Riedel M et al., 2002); b–interpretation profile showing the BSR within the accretionary wedge (after Westbrook GK et al., 1994).

thermogenic methane generation, migration, and accumulation as gas hydrate system over time.

5.1. Gas hydrate accumulation in inclined reservoirs in the Gulf of Mexico Basin

5.1.1. Geological model

The seismic profile at GC955 in the Gulf of Mexico shows high-amplitude anomalies which are interpreted as gas hydrate layers over gas or water (Fig. 8; Haines SS et al., 2017). Although no obvious focused fluid migration conduits have been observed, the up-bending low-amplitude and chaotic seismic reflections suggest there may develop folding and fracturing due to the location above the crest of a gas chimney (Rowan MG et al., 2020). The diapir-accompanied gas chimney may have contributed to the formation of high-amplitude gas hydrate layers above.

Based on the seismic and drilling data from the Gulf of Mexico data, the authors constructed a 2-D model which is ca. 10 km long and ca. 3500 m thick, with a 200 m × 5 m grid resolution (Fig. 9). The geological parameters are assigned according to previous studies (Haines SS et al., 2017), water depths ranging from 1650 m to 2200 m, a seafloor temperature of 4°C, a heat flux of 50 mW/m^2, the oldest sediments of 0.65 Ma and maximum dip angle of ca. 10°. Considering the GC955 drilling data, the authors constructed the stratigraphic model using variable lithological parameters such as sand-rich sediments (75% sandstone, 25% siltstone) and mud-rich sediments (50% mudstone, 50% siltstone) (Table 4).

In the Gulf of Mexico Basin, gas hydrate system is primarily characterized by biogenic gas sources (Frye M et al., 2008), thus only the biogenic hydrocarbon generation kinetic model was considered. The hydrocarbon generation kinetic model utilizes the Middelburg biogenic hydrocarbon generation model, where the hydrocarbon generation rate is related to the burial rate and burial age of the sediments. In mud-rich sediments, the total organic carbon (TOC) is 1%, and the hydrogen index (HI) is 300 mg HC/g TOC (Burton ZFM, 2022). In contrast, sand-rich sediments are not conducive to the preservation of organic matter, hence no

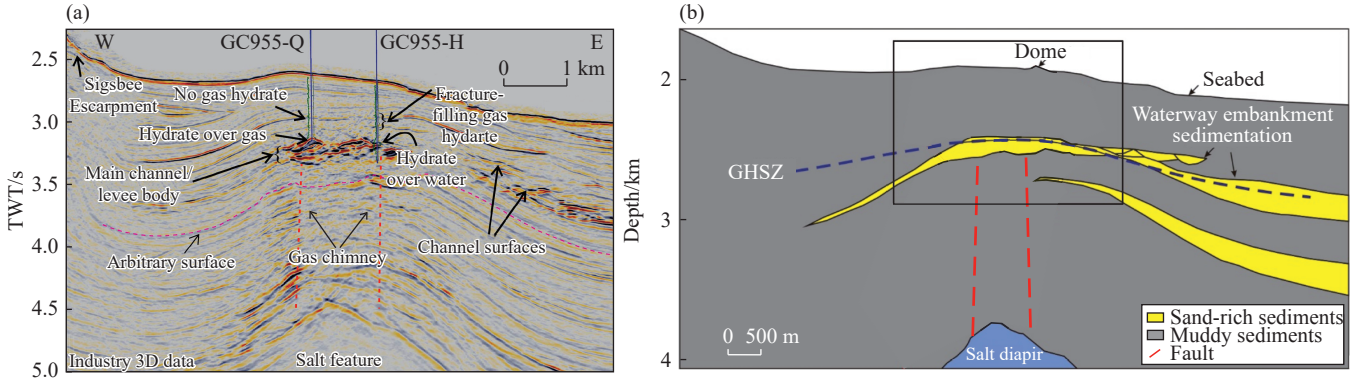


Fig. 8. Seismic profile (a) and interpretation profile pattern (b) of the Gulf of Mexico Basin (after Haines SS et al., 2017).

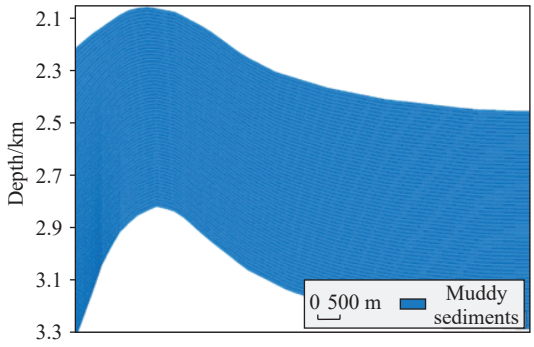


Fig. 9. Two–dimensional geological model based on the seismic profile in Fig. 8 from the Gulf of Mexico Basin.

TOC parameters are assigned. Additionally, in the fluid migration model, the Hybrid model is typically employed, which can be divided into various methods such as the Darcy migration mode (for low permeability formations), the Flowpath mode (for high permeability formations), and the fault migration mode. Three models have been built for the folded successions in the study area of Gulf of Mexico, homogeneous mud-rich sedimentary layers (Fig. 10a), interbedded mud-sand/silt layers without fluid migration conduits (Fig. 10d), and interbedded mud-sand/silt layers with gas chimney located at the crest of the folding (Fig. 10g).

5.1.2. Modeling results

For the homogeneous mud-rich model, Fig.10a illustrates the simulated migration of biogenic gas, which predominantly occurred within the shallow layers (< 200 m). Figs. 10b, c show the simulated hydrate saturation and free gas saturation, respectively, both of which showing limited distribution and low saturation. The simulated hydrate saturation is less than 15%, and there is almost no free gas existence below the BSR.

For the interbedded mud-sand/silt model without fluid migration conduits, the generated methane migrates from the mud layers into adjacent sand/silt layers, where buoyancy forces facilitate the up-dip migration of methane along the inclined successions (Fig. 10d). Compared with the homogeneous mud-rich model, lateral gas migration occurs both at shallow and comparatively deeper layers. Fig.10e shows that gas hydrate mainly forms above the BHSZ, with the maximum saturation reaching 50%. Within the GHSZ, the gas hydrate saturation is comparatively lower, but the maximum hydrate saturation above the structural high (the crest of the salt diapir, ca. 50%) is significantly higher than that on the flanks (ca. 20%). Fig.10f shows that multiple high-saturation free gas layers can form below the base of GHSZ, primarily distributed in the structural highs. Generally, both hydrate layers and free gas layers are predominantly located in sand-rich formations, particularly surrounding the structural high locations.

For the interbedded mud-sand/silt model with a gas chimney located at the crest of the folding, the simulated fluid migration is mainly featured by lateral up-dip migration of methane along the inclined sand/silt layers, and upward fluid migration has also been observed within the gas chimney structure (Fig. 10g). The simulated hydrate saturation result (Fig. 10h) shows that the distribution characteristics of low hydrate saturation (Fig. 10i) within the GHSZ are similar to the second model, but with higher-saturation hydrate layers above the structural high (the crest of the salt diapir). The saturation of free gas is much lower at the locations of gas chimney due to the presence of gas chimney, where the hydrate layers above the BHSZ increase markedly.

5.2. Gas hydrate accumulation in horizontal reservoirs in Qiongdongnan Basin

5.2.1. Geological model

Previous studies have established a detailed sequence stratigraphic framework of the sedimentary succession in Qiongdongnan Basin, with seven key reflections identified, T80 (33.9 Ma), T70 (28.4 Ma), T60 (23 Ma), T50 (16 Ma), T40 (11.6 Ma), T30 (5.5 Ma) and T20 (1.8 Ma) (Qiu N et al., 2013; Song GZ et al., 2014). Gas hydrate accumulations have been found in the Quaternary Ledong Formation (Fang XY et al., 2022). The seismic profile intersecting W08 Well in the Qiongdongnan Basin shows high-amplitude anomalies which are interpreted as gas hydrate system and mainly occur in successions shallower than T20 reflection which has been interpreted as the Quaternary Ledong Formation (Fig. 11; Fang XY et al., 2022). The gas hydrate system is spatially consistent with the basement uplift, and they are interconnected by vertical faults which may act as fluid

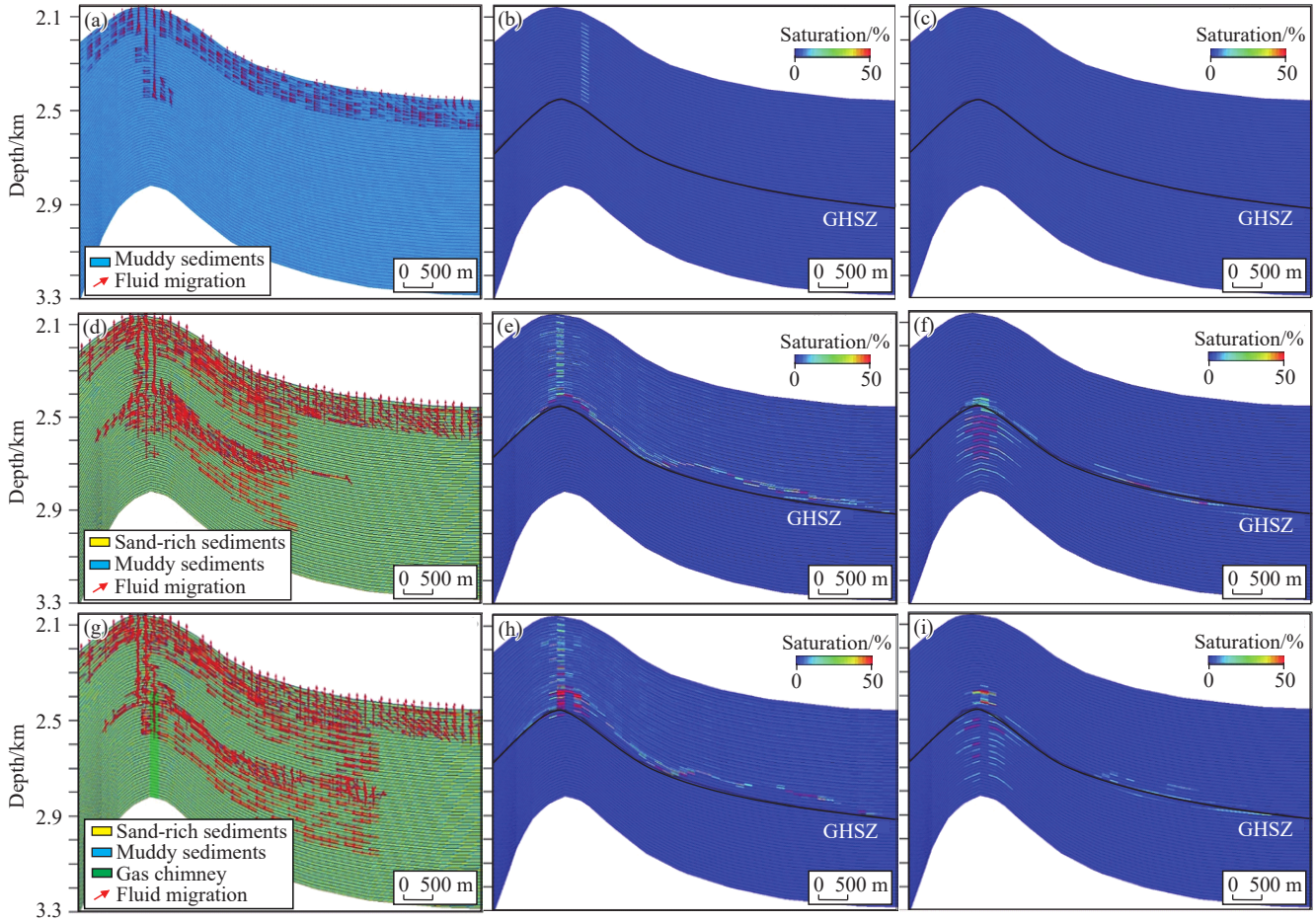


Fig. 10. Numerical modeling results of gas hydrate accumulation in the Gulf of Mexico Basin. a–Fluid transport for the homogeneous mudstone reservoirs; b–hydrate saturation for the homogeneous mudstone reservoirs; c–free gas saturation for the homogeneous mudstone reservoirs; d–fluid transport for the heterogeneous mud–sandstone reservoirs; e–hydrate saturation for the heterogeneous mud–sandstone reservoirs; f–free gas saturation for the heterogeneous mud–sandstone reservoirs; g–fluid transport for the heterogeneous mud–sandstone reservoirs and gas chimneys; h–hydrate saturation for the heterogeneous mud–sandstone reservoirs and gas chimneys; i–free gas saturation for the heterogeneous mud–sandstone reservoirs and gas chimneys.

migration conduits (Wang XJ et al., 2014). Other features such as central valley, polygonal faults and channel systems have been observed within the sedimentary successions (Xie X et al., 2003).

Based on the seismic and drilling data, the authors constructed a 2-D model which has a depth of ca. 1700 m below sea level, a width of ca. 35 km and a burial depth of ca. 2.5 km (Fig. 12). The authors have simplified the model by assuming horizontal strata to investigate the influence of stratum dip angles on fluid migration. Shallow Quaternary strata exhibit multi-stage channel and mass transport deposits, where sand-rich sediments could exist (Lai HF et al., 2021; He YL et al., 2022; Zuo TN et al., 2022). The shallow sedimentary successions (< 2000 m below the sea level) are predominantly horizontal. The Qiongdongnan Basin is influenced by Cenozoic lithospheric extension and Neotectonic movements, leading to crustal thinning in the continental slope and generally higher geothermal gradients, higher present-day temperatures, and higher heat flow values in the deep-water areas of the basin (Ye JL et al., 2019). Previous studies indicate that the average heat flow value in the northern shallow-water area is 70 mW/m^2, while the average heat flow value in the continental slope deep-water area is 85 mW/m^2 (Zhang YZ et al., 2019). In the initial heat flow model, only a constant heat flow value of 63 mW/m^2 at the time of basement formation (33.9 Ma) was considered. Drilling data from gas hydrate exploration reveal that the seafloor temperature is ca. 3.5°C, and both the initial and present-day seafloor temperatures are set at 3.5°C (Sun LY et al., 2023). The heat flow above basement uplift structures is relatively high, reaching up to 130 mW/m^2, while the heat flow in the flanking strata is around 70 mW/m^2 (Sun LY et al., 2023).

The gas origin of gas hydrate in the Qiongdongnan Basin is primarily thermogenic, but it may also include contributions from biogenic gas, exhibiting overall mixed genetic characteristics (Figs. 2, 3). Therefore, both biogenic and thermogenic hydrocarbon kinetics models have been considered in the modeling. The biogenic hydrocarbon kinetics model is similar to that of the Gulf of Mexico Basin, but with a total organic carbon (TOC) content of 0.5% and a hydrogen index (HI) value of 100 mg/g TOC (Burton ZFM, 2022). The thermogenic hydrocarbon kinetics model has been used for strata deeper than 1500 m below sea level, and it

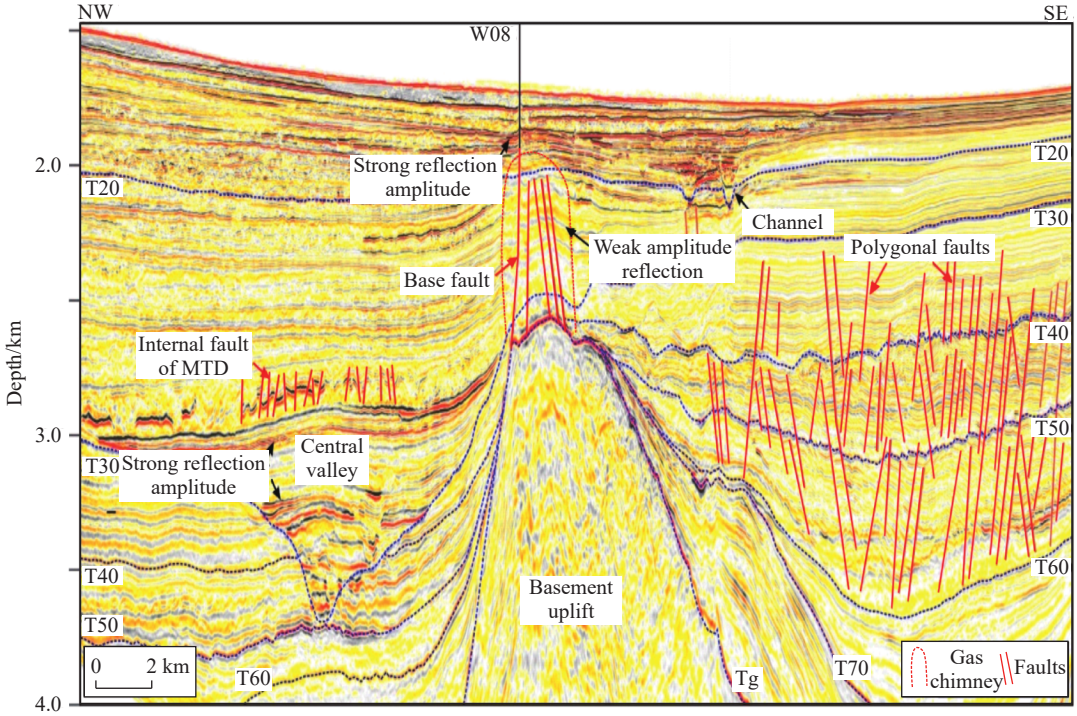


Fig. 11. Two-dimensional seismic profile of the Qiongdongnan Basin showing the structures and the shallow high-amplitude reflection indicating the presence of gas hydrate system (after Sun LY et al., 2023).

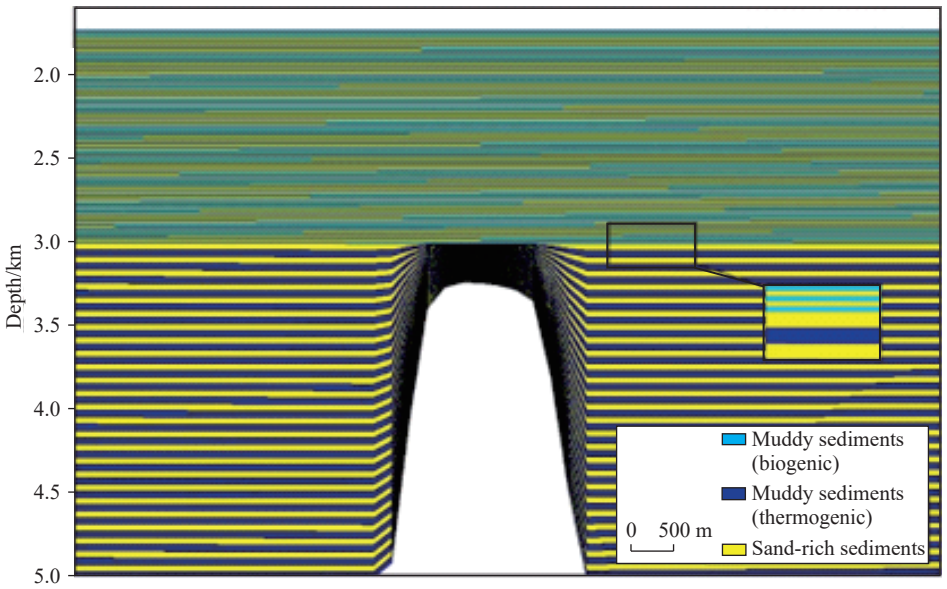


Fig. 12. Simplified sand-mud interbedded geological model based on the seismic profile in Fig. 11 in the Qiongdongnan Basin.

adopts the Burnham AK (1989) Type III model with a TOC value of 1% and an HI value of 200 mg/g TOC.

Two models are built to simulate the gas hydrate accumulation history in the Qiongdongnan Basin. Both are mud-sand interbedded lithology model, but only one develops fault structures above the basement uplift (Fig. 13). Using the same method as in the Gulf of Mexico Basin, the fluid migration pathways, hydrate and free gas saturations are simulated for the two geological models. Other lithology and physical parameters are the same as those used in the Gulf of Mexico Basin (Table 4).

5.2.2. Modeling results

For the interbedded mud-sand model without fluid migration conduits, Fig. 13a illustrates the simulated migration of both biogenic and thermogenic gas. It shows that biogenic gas migration mainly occurs in shallow subsurface probably because gas can migrate only when the driving force (buoyancy and residual pressure) surpasses the sum of the capillary resistance and the frictional resistance (Wang ZX, 2000). Thermogenic gas migration mainly occurs at depth deeper than 3500 m below sea level as there is limited generation of thermogenic gas above this depth as demonstrated by the modeling. The deeper thermogenic gas

has not been transported to the shallow GHSZ due to the absence of fluid migration conduits. Figs. 13b, c depict the simulated the saturations of hydrate and free gas, respectively, showing almost no distribution of gas hydrate or underneath free gas. Therefore, the authors propose that without deeper thermogenic gas origin (>1500 m), the *in-situ* biogenic gas is insufficient to form gas hydrate system in Qiongdongnan Basin.

For the interbedded mud-sand model with faults occurring above the basement uplift, Fig. 13d illustrates a two-stage gas migration mechanism. Primary gas migration occurs along the vertical faults which rooted in the uplift structure, channeling deeper thermogenic gas into the shallow sediments. Subsequently at the tops of the faults, gas can continue migrating upwards to the GHSZ along the shallow migration pattern which is similar to the first model. The simulated hydrate saturation result shows a gas hydrate saturation of ca. 40% above the BSR in the basement uplift region (Fig. 13e), and almost no free gas or very low saturation of free gas forms under the BSR (Fig. 13f). A low saturation of free gas (1%−3%) may cause a strong decrease of P-wave velocity and therefore forming high amplitude on seismic profiles (Berndt C et al., 2004).

6. Discussion

In this study, the authors highlight the importance of advective fluid migration in the formation and accumulation of either biogenic or mixed origin gas hydrate. Numerical modeling results in the Gulf of Mexico show that although the mud-rich lithology is favorable for the generation of biogenic gas, the lack of permeable sand layers and fluid migration conduits hinder the accumulations of gas hydrate and underlying free gas zone (Figs. 10a–c). By contract, the presence of inclined permeable sand layers (Figs. 10d–i) and gas chimney (Figs. 10g–i) facilitate the upward migration of deep fluids to the shallow GHSZ, forming the gas hydrate system. Based on 1-D numerical modeling, You KH et al. (2021) proposed that free gas flow plays a key role in transporting recycled methane and biogenic methane generated below the BHSZ. That is consistent with the proposal in this study that in the Gulf of Mexico, the *in-situ* biogenic gas is insufficient to form gas hydrate which needs allochthonous gas source, either biogenic or thermogenic origin (>1500 m). Similarly, the modeling results in Qiongdongnan Basin show that without deeper thermogenic gas origin, the *in-situ* biogenic gas is insufficient to form gas hydrate system, and external gas sources, either biogenic or thermogenic, are necessary to form favorable gas hydrate system which depend on the presence of fluid migration conduits (Fig. 13).

Additionally, 19 gas hydrate case studies are analyzed in this study to examine the spatial relationship between fluid migration pathways and natural gas hydrate systems (Table 2). It shows that most gas hydrate systems are spatially related with focused fluid migration conduits (mainly faults and gas chimneys), which enable upward migration of both thermogenic and biogenic gases from deeper or distant regions to the GHSZ (Fig. 14). Among these 19 regions, only two show no obvious fluid migration conduits: The Fiordland-Pusegur Margin of New Zealand (Crutchley GJ et al., 2007) and the Mid-Norwegian margin (Mienert J et al., 2022). The Fiordland-Pusegur Margin has remained underexplored owing to its geographical isolation, extreme climatic conditions, and limited potential for conventional hydrocarbon resources, and future availability of high-resolution seismic data may help better understand the gas hydrate system and related fluid migration pathways. Generally fluid migration conduits play a key role in gas hydrate accumulation by providing allochthonous biogenic or thermogenic gas to the GHSZ. The 2-D numerical modeling results in both Gulf of Mexico Basin and Qiongdongnan Basin have shown the significance of focused fluid migration conduits in forming high saturations of gas hydrate and underlying free gas, which strongly corroborated the findings of You KH et al. (2021) from different prospects.

Another key factor affecting the formation of gas hydrate system is the stratigraphy, and dipping strata composed of alternating mud and sand sediments are favorable for up-dip gas migration along layers of permeable coarser sand sediments. For example, in the Gulf of Mexico, the modeling results show formation of gas hydrate and free gas in the second and third geological models, both featured by folded interbedded mud-sand/silt layers. The inclined sand layers are potential fluid migration conduits which enable gas migration from deeper strata to the GHSZ. For the first model, the homogeneous mud-rich sedimentary layers inhibit gas migration due to the limited permeability. Additionally, the authors simplified the model in Qiongdongnan Basin by creating horizontal strata, and the modeling results show that there is no lateral gas migration along the horizontal sand layers. Some lateral gas migration occurs around the basement uplift region where the strata are inclined. Therefore, lithology and stratal dip are both important in affecting fluid migration, determining the formation of gas hydrate systems.

7. Conclusions

A comprehensive review of gas sources for global gas hydrate systems has been conducted in this study, including geochemical analysis of gas origins in 13 areas, geophysical investigation of the spatial relationship between the fluid migration pathways and natural gas hydrate systems in 19 case studies. Numerical simulations of the gas hydrate accumulation have also been carried out in Gulf of Mexico and Qingdongnan Basin which reveal the controlling factors of gas hydrate formation and underlying free gas accumulation. The key findings are as follows.

(i) Review of the genetic types of the hydrate-bound gas samples shows that mixed-origin gas accounts for approximately 55% of hydrate samples over the globe, biogenic origin accounts for 32%, and thermogenic origin accounts for 13%. For the gas hydrate of mixed origin, thermogenic gas may contribute more (e.g., Shenhu area), and biogenic gas may be reproduced by the secondary

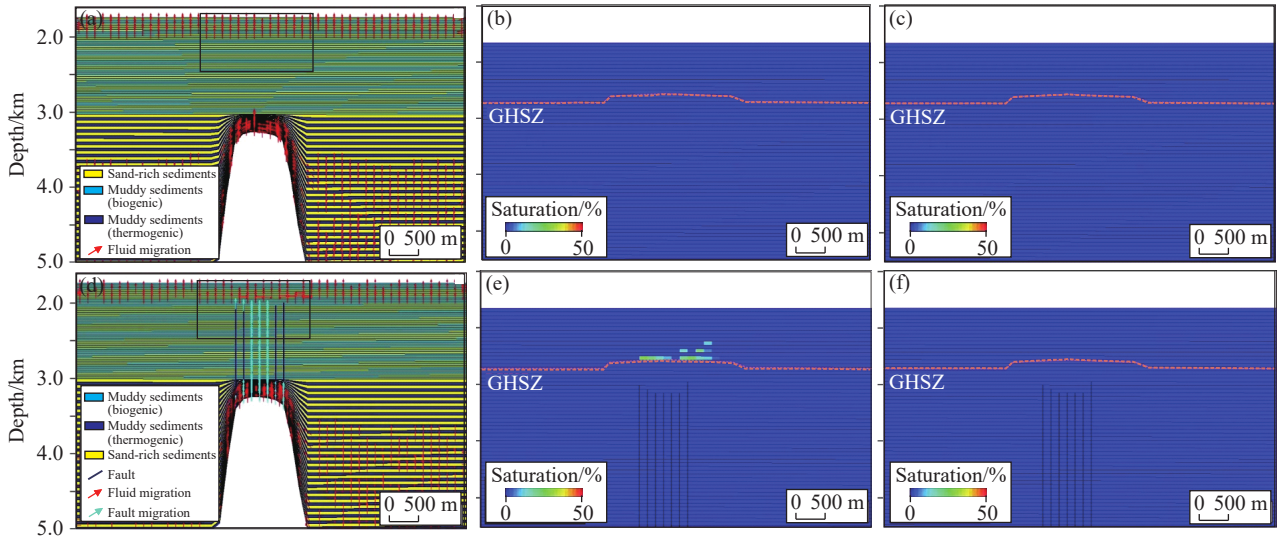


Fig. 13. Numerical modeling results of gas hydrate accumulation in the Qiongdongnan Basin. a–Fluid transport for the heterogeneous mud-sandstone reservoirs; b–hydrate saturation for the heterogeneous mud–sandstone reservoirs; c–free gas saturation for the heterogeneous mud–sandstone reservoirs; d–fluid transport for the heterogeneous mud–sandstone reservoirs and faults; e–hydrate saturation for the heterogeneous mud–sandstone reservoirs and faults; f–free gas saturation for the heterogeneous mud–sandstone reservoirs and faults.

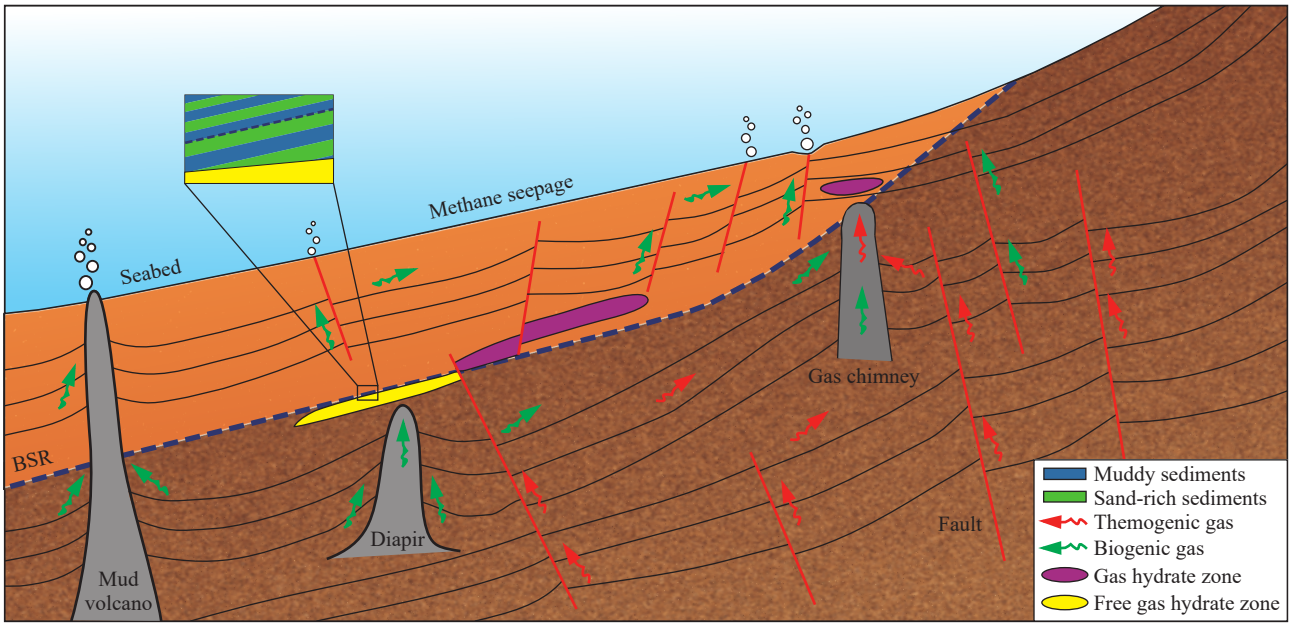


Fig. 14. Schematic diagram of the migration pathways of the gas hydrate system reviewed in this study. BSR−Bottom simulating reflector.

biodegradation of deeply-sourced thermogenic gas.

(ii) Seismic interpretation and numerical simulation in both Gulf of Mexico Basin and Qiongdongnan Basin show the significance of focused fluid migration conduits. It is proposed that the *in-situ* biogenic gas is insufficient to form potential gas hydrate systems, and fluid migration conduits are necessary to transport allochthonous biogenic or thermogenic gas to the GHSZ and form both gas hydrate and underlying free gas.

(iii) Comparison of the two numerical simulations shows that stratigraphy is another key parameter which affects the formation of gas hydrate systems. Alternating mud and sand layers are preferred for hydrate formation than homogeneous mud-rich sedimentary layers, and the inclination of sediment layers is conducive to lateral long-distance migration of methane. Therefore, lithology and stratal dip are both important in affecting fluid migration, playing key roles in the formation of gas hydrate systems.

CRediT authorship contribution statement

Jin-Xiu Yang, Chen Wang and Ang Li conceived of the presented idea, and carried out conceptualization. Chen Wang, Li Zhao and Kun-Yi Liu made the visualization and numerical modeling using software. All authors discussed the results and completed the writing and revising of manuscript.

Declaration of competing interest

The authors declare no conflicts of interest.

Acknowledgement

This research was supported by National Natural Science Foundation of China (42476070, 42376069), Taishan Scholar Project (TSQN202408292), National Engineering Research Center of Gas Hydrate Exploration and Development (NERCY [202401]) and Marine Geological Survey Program of China Geological Survey (DD20230402).

References

Bahk JJ, Kim JH, Kong GS, Park Y, Lee H, Park Y, Park KP. 2009. Occurrence of near–seafloor gas hydrates and associated cold vents in the Ulleung Basin, East Sea. Geosciences Journal, 13(4), 371–385. doi: 10.1007/s12303-009-0039-8.

Behrens EW. 1984. Unifite muds in intraslope basins, northwest Gulf of Mexico. Geo–Marine Letters, 4(3), 227–233. doi: 10.1007/BF02281711.

Benson TR, Coble MA, Rytuba JJ, Mahood GA. 2017. Lithium enrichment in intracontinental rhyolite magmas leads to Li deposits in caldera basins. Nature Communications, 8, 270. doi: 10.1038/s41467-017-00234-y.

Bernard B, Brooks JM, Sackett WM. 1977. A Geochemical Model For Characterization Of Hydrocarbon Gas Sources In Marine Sediments Offshore Technology Conference. May 1–4, 1977. Houston, Texas. OTC, 2934. doi: 10.4043/2934-ms.

Bernard BB, Brooks JM, Sackett WM. 1976. Natural gas seepage in the Gulf of Mexico. Earth and Planetary Science Letters, 31(1), 48–54. doi: 10.1016/0012-821X(76)90095-9.

Berndt C. 2005. Focused fluid flow in passive continental margins. Philosophical Transactions of the Royal Society A: Mathematical, Physical and Engineering Sciences, 363(1837), 2855–2871. doi: 10.1098/rsta.2005.1666.

Berndt C, Bünz S, Clayton T, Mienert J, Saunders M. 2004. Seismic character of bottom simulating reflectors: Examples from the mid–Norwegian margin. Marine and Petroleum Geology, 21(6), 723–733. doi: 10.1016/j.marpetgeo.2004.02.003.

Borowski WS. 2004. A review of methane and gas hydrates in the dynamic, stratified system of the Blake Ridge region, offshore southeastern North America. Chemical Geology, 205(3–4), 311–346. doi: 10.1016/j.chemgeo.2003.12.022.

Boswell R, Collett TS, Frye M, Shedd W, McConnell DR, Shelander D. 2012. Subsurface gas hydrates in the northern Gulf of Mexico. Marine and Petroleum Geology, 34(1), 4–30. doi: 10.1016/j.marpetgeo.2011.10.003.

Brocławik O, Bukawska–Matuszewska K, Brodecka–Goluch A, Bolałek J. 2020. Impact of methane occurrence on iron speciation in the sediments of the Gdansk Basin (Southern Baltic Sea). Science of the Total Environment, 721, 137718. doi: 10.1016/j.scitotenv.2020.137718.

Burnham AK. 1989. A simple kinetic model of petroleum formation and cracking. Lawrence Livermore National Laboratory Report UCID-21665, 11.

Burton ZFM. 2022. Sediment organic contents required for gas hydrate formation: A survey of published basin and hydrocarbon system models. Fuels, 3(4), 580–587. doi: 10.3390/fuels3040035.

Cartwright J, Huuse M, Aplin A. 2007. Seal bypass systems. AAPG Bulletin, 91(8), 1141–1166. doi: 10.1306/04090705181.

Chen DX, Wu SG, Dong DD, Mi LJ, Fu SY, Shi HS. 2013. Focused fluid flow in the Baiyun Sag, northern South China Sea: Implications for the source of gas in hydrate reservoirs. Chinese Journal of Oceanology and Limnology, 31(1), 178–189. doi: 10.1007/s00343-013-2075-5.

Chen SC, Hsu SK, Wang YS, Chung SH, Chen PC, Tsai CH, Liu CS, Lin HS, Lee YW. 2014. Distribution and characters of the mud diapirs and mud volcanoes off southwest Taiwan. Journal of Asian Earth Sciences, 92, 201–214. doi: 10.1016/j.jseaes.2013.10.009.

Choi J, Kim JH, Torres ME, Hong WL, Lee JW, Yi BY, Bahk JJ, Lee KE. 2013. Gas origin and migration in the Ulleung Basin, East Sea: Results from the Second Ulleung Basin Gas Hydrate Drilling Expedition (UBGH2). Marine and Petroleum Geology, 47, 113–124. doi: 10.1016/j.marpetgeo.2013.05.022.

Chung HM, Gormly JR, Squires RM. 1988. Origin of gaseous hydrocarbons in subsurface environments: Theoretical considerations of carbon isotope distribution. Chemical Geology, 71(1–3), 97–104. doi: 10.1016/0009-2541(88)90108-8.

Collett TS, Boswell R, Waite WF, Kumar P, Roy SK, Chopra K, Singh SK, Yamada Y, Tenma N, Pohlman J, Zyrianova M. 2019. India National Gas Hydrate Program Expedition 02 Summary of Scientific Results: Gas hydrate systems along the eastern continental margin of India. Marine and Petroleum Geology, 108, 39–142. doi: 10.1016/j.marpetgeo.2019.05.023.

Collett TS, Johnson A, Knapp CC, Boswell R. 2010. Natural gas hydrates: Energy resource potential and associated geologic hazards. AAPG Memoir 89, 781. doi: 10.1306/M891320.

Coren F, Volpi V, Tinivella U. 2001. Gas hydrate physical properties imaging by multi–attribute analysis—Blake Ridge BSR case history. Marine Geology, 178(1), 197–210. doi: 10.1016/S0025-3227(01)00156-6.

Crutchley GJ, Gorman AR, Fohrmann M. 2007. Investigation of the role of gas hydrates in continental slope stability west of Fiordland, New Zealand. New Zealand Journal of Geology and Geophysics, 50(4), 357–364. doi: 10.1080/00288300709509842.

Dai JC, Xu HB, Snyder F, Dutta N. 2004. Detection and estimation of gas hydrates using rock physics and seismic inversion: Examples from the northern deepwater Gulf of Mexico. The Leading Edge, 23(1), 60–66. doi: 10.1190/1.1645456.

Dai JX, Ni YY, Huang SP, Peng WL, Han WX, Gong DY, Wei W. 2017. Genetic types of gas hydrates in China. Petroleum Exploration and Development, 44(6), 887–898. doi: 10.1016/S1876-3804(17)30101-5.

Dai JX, Zou CN, Zhang SC, Li J, Ni YY, Hu GY, Luo X, Tao SZ, Zhu GY, Mi JK, Li ZS, Hu AP, Yang C, Zhou QH, Shuai YH, Zhang Y, Ma CH. 2008. Discrimination of abiogenic and biogenic alkane gases. Science in China Series D: Earth Sciences, 51, 1737–1749. doi: 10.1007/s11430-008-0133-1.

Etiope G, Baciu CL, Schoell M. 2011. Extreme methane deuterium, nitrogen and helium enrichment in natural gas from the Homorod seep (Romania). Chemical Geology, 280(1–2), 89–96. doi: 10.1016/j.chemgeo.2010.10.019.

Davies RJ, Yang JX, Ireland MT, Berndt C, Maqueda MÁM, Huuse M. 2024. Long–distance migration and venting of methane from the base of the hydrate stability zone. Nature Geoscience, 17(1), 32–37. doi: 10.1038/s41561-023-01333-w.

Fang XY, Yao Z, Liao J, Ge JW, Zhao XM, Song P, Xiang Z, Ma C. 2022. Sequence stratigraphic architecture of the Quaternary Ledong Formation in the deep–water area of the Qiongdongnan Basin and its significance to gas hydrate exploration. Marine Geology Frontiers, 38(1), 51–60 (in Chinese with English abstract). doi: 10.16028/j.1009-2722.2021.121.

Frye M, Grace J, Hunt J, Kaufman G, Schuenemeyer J, Shedd W. 2008. Methane Hydrate Resource Assessment of the Outer Continental Shelf: In–Place Gulf of Mexico Results.

Fu C, Yu XH, He LY, Liang JQ, Kuang ZG. 2019. Different initial density turbidite sediments with coarse grain injection and their corresponding flow pattern: Additional insights from numerical simulation in a study case of South China Sea. Petroleum Research,

4(1), 19–28. doi: 10.1016/j.ptlrs.2018.12.001.

Fu SY, Lu JA. 2010. The characteristics and origin of gas hydrate in Shenhu area, South China Sea. Marine Geology Letters, 26(9), 6–10 (in Chinese with English abstract). doi: 10.16028/j.1009-2722.2010.09.008.

Gay A, Berndt C. 2007. Cessation/reactivation of polygonal faulting and effects on fluid flow in the Vøring Basin, Norwegian Margin. Journal of the Geological Society, 164(1), 129–141. doi: 10.1144/0016-76492005-178.

Gay A, Lopez M, Berndt C, Séranne M. 2007. Geological controls on focused fluid flow associated with seafloor seeps in the Lower Congo Basin. Marine Geology, 244(1–4), 68–92. doi: 10.1016/j.margeo.2007.06.003.

Haacke RR, Hyndman RD, Park KP, Yoo DG, Stoian I, Schmidt U. 2009. Migration and venting of deep gases into the ocean through hydrate–choked chimneys offshore Korea. Geology, 37(6), 531–534. doi: 10.1130/G25681A.1.

Hachikubo A, Yanagawa K, Tomaru H, Lu HL, Matsumoto R. 2015. Molecular and isotopic composition of volatiles in gas hydrates and in sediment from the Joetsu Basin, eastern margin of the Japan Sea. Energies, 8(6), 4647–4666. doi: 10.3390/en8064647.

Haacke RR, Westbrook GK, Hyndman RD. 2007. Gas hydrate, fluid flow and free gas: Formation of the bottom–simulating reflector. Earth and Planetary Science Letters, 261(3–4), 407–420. doi: 10.1016/j.epsl.2007.07.008.

Haines SS, Hart PE, Collett TS, Shedd W, Frye M, Weimer P, Boswell R. 2017. High–resolution seismic characterization of the gas and gas hydrate system at Green Canyon 955, Gulf of Mexico, USA. Marine and Petroleum Geology, 82(4), 220–237. doi: 10.1016/j.marpetgeo.2017.01.029.

Han WC, Chen LW, Liu CS. 2021. Distribution and characteristics of gas chimneys in the passive margin offshore SW Taiwan. Marine Geophysical Research, 42(3), 25. doi: 10.1007/s11001-021-09447-9.

He YL, Liang JQ, Kuang ZG, Deng W, Ren JF, Lai HF, Meng MM, Zhang W. 2022. Migration and accumulation characteristics of natural gas hydrates in the uplifts and their slope zones in the Qiongdongnan Basin, China. China Geology, 5(2), 234–250. doi: 10.31035/cg2022004.

Hillman JIT, Cook AE, Daigle H, Nole M, Malinverno A, Meazell K, Flemings PB. 2017. Gas hydrate reservoirs and gas migration mechanisms in the Terrebonne Basin, Gulf of Mexico. Marine and Petroleum Geology, 86, 1357–1373. doi: 10.1016/j.marpetgeo.2017.07.029.

Hornbach MJ, Saffer DM, Holbrook WS. 2004. Critically pressured free-gas reservoirs below gas-hydrate provinces. Nature, 427(6970), 142–144. doi: 10.1038/nature02172.

Horozal S, Kim GY, Cukur D, Bahk JJ, Buchs D, Ryu BJ, Lee GH, Kim SP. 2017. Sedimentary and structural evolution of the Eastern South Korea Plateau (ESKP), East Sea (Japan Sea). Marine and Petroleum Geology, 85, 70–88. doi: 10.1016/j.marpetgeo.2017.04.014.

Horozal S, Lee GH, Yi BY, Yoo DG, Park KP, Lee HY, Kim W, Kim HJ, Lee K. 2009. Seismic indicators of gas hydrate and associated gas in the Ulleung Basin, East Sea (Japan Sea) and implications of heat flows derived from depths of the bottom–simulating reflector. Marine Geology, 258(1–4), 126–138. doi: 10.1016/j.margeo.2008.12.004.

Hsu HH, Liu CS, Chang YT, Chang JH, Ko CC, Chiu SD, Chen SC. 2017. Diapiric activities and intraslope basin development offshore of SW Taiwan: A case study of the Lower Fangliao Basin gas hydrate prospect. Journal of Asian Earth Sciences, 149, 145–159. doi: 10.1016/j.jseaes.2017.05.007.

Hutchinson DR, Hart PE, Ruppel CD, Snyder F, Dugan B. 2009. Seismic and thermal characterization of a bottom-simulating reflection in the northern Gulf of Mexico. Natural Gas Hydrates—Energy Resource Potential and Associated Geologic Hazards. Tulsa: American Association of Petroleum Geologists, 266–286. doi: 10.1306/13201146m893343.

Inks TL, Lee MW, Agena WF, Taylor DJ, Collett TS, Zyrianova MV, Hunter RB. 2009. Seismic prospecting for gas-hydrate and associated free-gas prospects in the Milne point area of northern Alaska. Natural Gas Hydrates—Energy Resource Potential and Associated Geologic Hazards. Tulsa: American Association of Petroleum Geologists, 555–583. doi: 10.1306/13201164m893360.

Jin JP, Wang XJ, Guo YQ, Li J, Li YP, Zhang X, Qian J, Sun LY. 2020. Geological controls on the occurrence of recently formed highly concentrated gas hydrate accumulations in the Shenhu area, South China Sea. Marine and Petroleum Geology, 116(7), 104294. doi: 10.1016/j.marpetgeo.2020.104294.

Judd A, Hovland M. 2009. Seabed fluid flow: The impact on geology, biology and the marine environment. Cambridge, Cambridge University Press.

Kida M, Jin Y, Watanabe M, Konno Y, Yoneda J, Egawa K, Ito T, Nakatsuka Y, Suzuki K, Fujii T, Nagao J. 2015. Chemical and crystallographic characterizations of natural gas hydrates recovered from a production test site in the eastern Nankai Trough. Marine and Petroleum Geology, 66, 396–403. doi: 10.1016/j.marpetgeo.2015.02.019.

Kim JH, Park MH, Chun JH, Lee JY. 2011. Molecular and isotopic signatures in sediments and gas hydrate of the central/southwestern Ulleung Basin: high alkalinity escape fuelled by biogenically sourced methane. Geo–Marine Letters, 31(1), 37–49. doi: 10.1007/s00367-010-0214-y.

Kim JH, Torres ME, Choi J, Bahk JJ, Park MH, Hong WL. 2012. Inferences on gas transport based on molecular and isotopic signatures of gases at acoustic chimneys and background sites in the Ulleung Basin. Organic Geochemistry, 43(1), 26–38. doi: 10.1016/j.orggeochem.2011.11.004.

Kim JH, Torres ME, Hong WL, Choi J, Riedel M, Bahk JJ, Kim SH. 2013. Pore fluid chemistry from the Second Gas Hydrate Drilling Expedition in the Ulleung Basin (UBGH2): Source, mechanisms and consequences of fluid freshening in the central part of the Ulleung Basin, East Sea. Marine and Petroleum Geology, 47, 99–112. doi: 10.1016/j.marpetgeo.2012.12.011.

Kopf AJ. 2002. Significance of mud volcanism. Reviews of geophysics, 40(2), 1–2. doi: 10.1029/2000RG000093.

Krooss BM, Leythaeuser D, Schaefer RG. 1988. Light hydrocarbon diffusion in a caprock. Chemical Geology, 71(1–3), 65–76. doi: 10.1016/0009-2541(88)90106-4.

Lai HF, Fang YX, Kuang ZG, Ren JF, Liang JQ, Lu JA, Wang GL, Xing CZ. 2021. Geochemistry, origin and accumulation of natural gas hydrates in the Qiongdongnan Basin, South China Sea: Implications from site GMGS5–W08. Marine and Petroleum Geology, 123, 104774. doi: 10.1016/j.marpetgeo.2020.104774.

Lee MW, Collett TS. 2009. Gas hydrate saturations estimated from fractured reservoir at Site NGHP-01-10, Krishna-Godavari Basin, India. Journal of Geophysical Research: Solid Earth, 114(B7), B07102. doi: 10.1029/2008jb006237.

Lei C, Ren JY, Clift PD, Wang ZF, Li XS, Tong CX. 2011. The structure and formation of diapirs in the yinggehai–song hong basin, south China sea. Marine and Petroleum Geology, 28(5), 980–991. doi: 10.1016/j.marpetgeo.2011.01.001.

Leythaeuser D, Schaefer RG, Yukler A. 1982. Role of diffusion in primary migration of hydrocarbons. AAPG Bulletin, 66(4), 408–429. doi: 10.1306/03b59b2a-16d1-11d7-8645000102c1865d.

Li YY, Chang JY, Lu HL. 2022. Geochemical characteristics of gases associated with natural gas hydrate. Frontiers in Marine Science, 9, 968647. doi: 10.3389/FMARS.2022.968647.

Liang JQ, Zhang W, Lu JA, Wei JG, Kuang ZG, He YL. 2019.

Geological occurrence and accumulation mechanism of natural gas hydrates in the eastern Qiongdongnan Basin of the South China Sea: Insights from site GMGS5–W9–2018. Marine Geology, 418(1), 106042. doi: 10.1016/j.margeo.2019.106042.

Liang QY, Xiao X, Zhao J, Zhang W, Li Y, Wu XM, Ye JL, Qin XW, Qiu HJ, Liang JQ, Lu JA, Dong YF, Zhang TT, Xiong YQ, Jiang WM, Guo BB. 2022. Geochemistry and sources of hydrate–bound gas in the Shenhu area, northern South China Sea: Insights from drilling and gas hydrate production tests. Journal of Petroleum Science and Engineering, 208(3), 109459. doi: 10.1016/j.petrol.2021.109459.

Lin LF, Liu CS, Berndt C, Hsu HH, Wang Y, Chen SC. 2022. Gas Hydrate and Fluid–Related Seismic Indicators Across the Passive and Active Margins off SW Taiwan. World Atlas of Submarine Gas Hydrates in Continental Margins. Cham, Springer International Publishing, 173–181. doi: 10.1007/978-3-030-81186-0_14.

Liu CL, Meng QG, He XL, Li CF, Ye YG, Zhang GX, Liang JQ. 2015. Characterization of natural gas hydrate recovered from Pearl River Mouth basin in South China Sea. Marine and Petroleum Geology, 61, 14–21. doi: 10.1016/j.marpetgeo.2014.11.006.

Liu QY, Wu XQ, Wang XF, Jin ZJ, Zhu DY, Meng QQ, Huang SP, Liu JY, Fu Q. 2019. Carbon and hydrogen isotopes of methane, ethane, and propane: A review of genetic identification of natural gas. Earth–Science Reviews, 190, 247–272. doi: 10.1016/j.earscirev.2018.11.017.

Manger GE. 1963. Porosity and bulk density of sedimentary rocks. USGPO, 1963.

Martini AM, Walter LM, Budai JM, Ku TC, Kaiser CJ, Schoell M. 1998. Genetic and temporal relations between formation waters and biogenic methane: Upper Devonian Antrim Shale, Michigan Basin, USA. Geochimica et Cosmochimica Acta, 62(10), 1699–1720. doi: 10.1016/S0016-7037(98)00090-8.

Maillard A, Gaullier V, Vendeville BC, Odonne F. 2003. Influence of differential compaction above basement steps on salt tectonics in the Ligurian–Provençal Basin, northwest Mediterranean. Marine and Petroleum Geology, 20(1), 13–27. doi: 10.1016/S0264-8172(03)00022-9.

Mienert J, Tréhu AM, Berndt C, Camerlenghi A, Liu CS, Massironi M. 2022. Finding and using the world's gas hydrates. World Atlas of Submarine Gas Hydrates in Continental Margins. Cham, Springer International Publishing, 33–52. doi: 10.1007/978-3-030-81186-0_3.

Milkov AV. 2005. Molecular and stable isotope compositions of natural gas hydrates: A revised global dataset and basic interpretations in the context of geological settings. Organic Geochemistry, 36(5), 681–702. doi: 10.1016/j.orggeochem.2005.01.010.

Milkov AV. 2011. Worldwide distribution and significance of secondary microbial methane formed during petroleum biodegradation in conventional reservoirs. Organic Geochemistry, 42(2), 184–207. doi: 10.1016/j.orggeochem.2010.12.003.

Milkov AV, Claypool GE, Lee YJ, Sassen R. 2005. Gas hydrate systems at Hydrate Ridge offshore Oregon inferred from molecular and isotopic properties of hydrate-bound and void gases. Geochimica et Cosmochimica Acta, 69(4), 1007–1026 doi: 10.1016/j.gca.2004.08.021.

Milkov AV, Etiope G. 2018. Revised genetic diagrams for natural gases based on a global dataset of > 20, 000 samples. Organic Geochemistry, 125, 109–120. doi: 10.1016/j.orggeochem.2018.09.002.

Miller DJ, Ketzer JM, Viana AR, Kowsmann RO, Freire AFM, Oreiro SG, Augustin AH, Lourega RV, Rodrigues LF, Heemann R, Preissler AG, Machado CX, Sbrissa GF. 2015. Natural gas hydrates in the Rio Grande Cone (Brazil): A new province in the western South Atlantic. Marine and Petroleum Geology, 67, 187–196. doi: 10.1016/j.marpetgeo.2015.05.012.

Nakajima T, Kakuwa Y, Yasudomi Y, Itaki T, Motoyama I, Tomiyama T, Machiyama H, Katayama H, Okitsu O, Morita S, Tanahashi M, Matsumoto R. 2014. Formation of pockmarks and submarine canyons associated with dissociation of gas hydrates on the Joetsu Knoll, eastern margin of the Sea of Japan. Journal of Asian Earth Sciences, 90, 228–242 doi: 10.1016/j.jseaes.2013.10.011.

Ojha M, Sain K. 2009. Seismic attributes for identifying gas-hydrates and free-gas zones: Application to the Makran accretionary prism. Episodes, 32(4), 264–270. doi: 10.18814/epiiugs/2009/v32i4/003.

Paganoni M, Cartwright JA, Foschi M, Shipp CR, Van Rensbergen P. 2018. Relationship between fluid–escape pipes and hydrate distribution in offshore Sabah (NW Borneo). Marine Geology, 395, 82–103. doi: 10.1016/j.margeo.2017.09.010.

Palodkar AV, Jana AK. 2017. Formulating formation mechanism of natural gas hydrates. Scientific Reports, 7(1), 6392. doi: 10.1038/s41598-017-06717-8.

Pohlman JW, Canuel EA, Chapman NR, Spence GD, Whiticar MJ, Coffin RB. 2005. The origin of thermogenic gas hydrates on the northern Cascadia Margin as inferred from isotopic ($^{13}C/^{12}C$ and D/H) and molecular composition of hydrate and vent gas. Organic Geochemistry, 36(5), 703–716. doi: 10.1016/j.orggeochem.2005.01.011.

Pohlman JW, Kaneko M, Heuer VB, Coffin RB, Whiticar M. 2009. Methane sources and production in the northern Cascadia margin gas hydrate system. Earth and Planetary Science Letters, 287(3), 504–512. doi: 10.1016/j.epsl.2009.08.037.

Priest JA, Rees EVL, Clayton CRI. 2009. Influence of gas hydrate morphology on the seismic velocities of sands. Journal of Geophysical Research: Solid Earth, 114(B11), 2009JB006284. doi: 10.1029/2009jb006284.

Qian J, Wang XJ, Collett TS, Guo YQ, Kang DJ, Jin JP. 2018. Downhole log evidence for the coexistence of structure II gas hydrate and free gas below the bottom simulating reflector in the South China Sea. Marine and Petroleum Geology, 98, 662–674. doi: 10.1016/j.marpetgeo.2018.09.024.

Qiu N, Wang ZF, Xie H, Sun ZP, Wang ZW, Sun Z, Zhou D. 2013. Geophysical investigations of crust–scale structural model of the Qiongdongnan Basin, Northern South China Sea. Marine Geophysical Research, 34(3–4), 259–279. doi: 10.1007/s11001-013-9182-8.

Ren JF, Cheng C, Jiang T, Kuang ZG, Lai HF, Liang JQ, Chen ZG, Li T. 2023. Faults and gas chimneys jointly dominate the gas hydrate accumulation in the Shenhu Area, northern South China Sea. Frontiers in Marine Science, 10, 1254410. doi: 10.3389/FMARS.2023.1254410.

Ren JF, Qiu HJ, Kuang ZG, Li TW, He YL, Xu MJ, Wang XX, Lai HF, Liang J. 2024. Deep-large faults controlling on the distribution of the venting gas hydrate system in the middle of the Qiongdongnan Basin, South China Sea. China Geology, 7(1), 36–50. doi: 10.31035/cg2023086.

Riedel M, Collett TS, Kumar P, Sathe AV, Cook A. 2010. Seismic imaging of a fractured gas hydrate system in the Krishna–Godavari Basin offshore India. Marine and Petroleum Geology, 27(7), 1476–1493. doi: 10.1016/j.marpetgeo.2010.06.002.

Riedel M, Collett TS, Scherwath M, Pohlman JW, Hyndman R, Spence G. 2022. Northern Cascadia Margin Gas Hydrates —Regional Geophysical Surveying, IODP Drilling Leg 311 and Cabled Observatory Monitoring. World Atlas of Submarine Gas Hydrates in Continental Margins. Cham, Springer International Publishing, 109–120. doi: 10.1007/978-3-030-81186-0_8.

Riedel M, Spence GD, Chapman NR, Hyndman RD. 2002. Seismic investigations of a vent field associated with gas hydrates, offshore Vancouver Island. Journal of Geophysical Research: Solid Earth, 107(B9), 1–5. doi: 10.1029/2001JB000269.

Rincón-Martínez D, Ruge SM, Silva Arias A. 2022. Seismic analysis of the geological occurrence of gas hydrate in the Colombian Caribbean offshore. Journal of South American Earth Sciences, 116, 103800. doi: 10.1016/j.jsames.2022.103800.

Rodrigo C, Vera E, González–Fernández A. 2009. Seismic analysis and distribution of a bottom–simulating reflector (BSR) in the Chilean margin offshore of Valdivia (40°S). Journal of South American Earth Sciences, 27(1), 1–10. doi: 10.1016/j.jsames.2008.11.001.

Rowan MG, Muñoz JA, Giles KA, Roca E, Hearon Iv TE, Fiduk JC, Ferrer O, Fischer MP. 2020. Folding and fracturing of rocks adjacent to salt diapirs. Journal of Structural Geology, 141, 104187. doi: 10.1016/j.jsg.2020.104187.

Ruppel CD, Kessler JD. 2017. The interaction of climate change and methane hydrates. Reviews of Geophysics, 55(1), 126–168. doi: 10.1002/2016RG000534.

Sain K, Gupta H. 2012. Gas hydrates in India: Potential and development. Gondwana Research, 22(2), 645–657. doi: 10.1016/j.gr.2012.01.007.

Satyavani N, Sain K. 2015. Seismic insights into bottom simulating reflection (BSR) in the Krishna-Godavari Basin, eastern margin of India. Marine Georesources & Geotechnology, 33(3), 191–201. doi: 10.1080/1064119X.2013.797059.

Schmidt M, Hensen C, Mörz T, Müller C, Grevemeyer I, Wallmann K, Mau S, Kaul N. 2005. Methane hydrate accumulation in "Mound 11" mud volcano, Costa Rica forearc. Marine Geology, 216(1–2), 83–100. doi: 10.1016/j.margeo.2005.01.001.

Sarhan MA. 2023. Interpretation of diapiric structures and their effect on hydrocarbon prospects based on seismic data. Euro–Mediterranean Journal for Environmental Integration, 8(3), 637–644. doi: 10.1007/S41207-023-00383-1.

Schoell M, Faber E, Coleman ML. 1983. Carbon and hydrogen isotopic compositions of the NBS 22 and NBS 21 stable isotope reference materials: An inter–laboratory comparison. Organic Geochemistry, 5(1), 3–6. doi: 10.1016/0146-6380(83)90010-4.

Schofield N, Jolley DW. 2013. Development of intra–basaltic lava–field drainage systems within the Faroe-Shetland Basin. Petroleum Geoscience, 19(3), 273–288. doi: 10.1144/petgeo2012-061.

Schwalenberg K, Wood W, Pecher I, Hamdan L, Henrys S, Jegen M, Coffin R. 2010. Preliminary interpretation of electromagnetic, heat flow, seismic, and geochemical data for gas hydrate distribution across the Porangahau Ridge, New Zealand. Marine Geology, 272(1–4), 89–98. doi: 10.1016/j.margeo.2009.10.024.

Sherwood OA, Travers PD, Dolan MP. 2013. Compound-specific stable isotope analysis of natural and produced hydrocarbon gases surrounding oil and gas operations. Advanced Techniques in Gas Chromatography–Mass Spectrometry (GC–MS–MS and GC–TOF–MS) for Environmental Chemistry. Amsterdam: Elsevier, 347–372. doi: 10.1016/b978-0-444-62623-3.00015-0.

Shipley TH, Houston MH, Buffler RT, Shaub FJ, McMillen KJ, Laod JW, Worzel JL. 1979. Seismic evidence for widespread possible gas hydrate horizons on continental slopes and rises. AAPG Bulletin, 63(12), 2204–2213. doi: 10.1306/2f91890a-16ce-11d7-8645000102c1865d.

Song GZ, Wang H, Gan HJ, Sun ZP, Liu XL, Xu M, Ren JF, Sun M, Sun D. 2014. Paleogene tectonic evolution controls on sequence stratigraphic patterns in the central part of deepwater area of Qiongdongnan basin, northern South China Sea. Journal of Earth Science, 25(2), 275–288. doi: 10.1007/s12583-014-0433-7.

Stewart SA. 2006. Implications of passive salt diapir kinematics for reservoir segmentation by radial and concentric faults. Marine and Petroleum Geology, 23(8), 843–853. doi: 10.1016/j.marpetgeo.2006.04.001.

Su M, Sha ZB, Zhang CM, Wang HB, Wu NY, Yang R, Liang JQ, Qiao SH, Cong XR, Liu J. 2017. Types, characteristics and significances of migrating pathways of gas-bearing fluids in the Shenhu area, northern continental slope of the South China Sea. Acta Geologica Sinica (English Edition), 91(1), 219–231. doi: 10.1111/1755-6724.13073.

Su M, Yang R, Wang H, Sha ZB, Liang JH, Wu NY, Qiao SH, Cong XR. 2016. Gas hydrates distribution in the Shenhu area, northern South China Sea: comparisons between the eight drilling sites with gas–hydrate petroleum system. Geologica Acta, 14(2), 79–100. doi: 10.1344/GeologicaActa2016.14.2.1.

Su M, Yang R, Wu NY, Wang HB, Liang JQ, Sha ZB, Cong XR, Qiao SH. 2014. Structural characteristics in the Shenhu area, northern continental slope of South China Sea, and their influences on gas hydrate. Acta Geologica Sinica, 88(3), 318–326 (in Chinese with English abstract). doi: 10.19762/j.cnki.dizhixuebao.2014.03.002.

Sun LY, Li QP, Chen F, Yu H, Wang XJ, Jin JP, Qian J, Li LX, Zhang GX, Zhang ZY. 2023. The numerical modeling analysis on the characteristics of multi–type gas hydrates occurrence in the mass transport deposit area, the Qiongdongnan Basin. Chinese Journal of Geophysics, 66(11), 4721–4741 (in Chinese with English abstract). doi: 10.6038/cjg2023R0003.

Sun LY, Wang XJ, He M, Jin JP, Li J, Li YP, Zhu ZY, Zhang GX. 2020. Thermogenic gas controls high saturation gas hydrate distribution in the Pearl River Mouth Basin: Evidence from numerical modeling and seismic anomalies. Ore Geology Reviews, 127, 103846. doi: 10.1016/j.oregeorev.2020.103846.

Sun QL, Alves T, Xie XN, He JX, Li W, Ni XL. 2017. Free gas accumulations in basal shear zones of mass–transport deposits (Pearl River Mouth Basin, South China Sea): An important geohazard on continental slope basins. Marine and Petroleum Geology, 81, 17–32. doi: 10.1016/j.marpetgeo.2016.12.029.

Sun QL, Wu SG, Cartwright J, Dong DD. 2012. Shallow gas and focused fluid flow systems in the Pearl River Mouth Basin, northern South China Sea. Marine Geology, 315–318, 1–14. doi: 10.1016/j.margeo.2012.05.003.

Sun QL, Wu SG, Cartwright J, Wang SH, Lu YT, Chen DX, Dong DD. 2014. Neogene igneous intrusions in the northern South China Sea: Evidence from high-resolution three dimensional seismic data. Marine and Petroleum Geology, 54, 83–95. doi: 10.1016/j.marpetgeo.2014.02.014.

Trusheim F. 1960. Mechanism of salt migration in northern Germany. AAPG Bulletin, 44(9), 1519–1540. doi: 10.1306/0bda61ca-16bd-11d7-8645000102c1865d.

Van Rensbergen P, Morley CK, Ang DW, Hoan TQ, Lam NT. 1999. Structural evolution of shale diapirs from reactive rise to mud volcanism: 3D seismic data from the Baram delta, offshore Brunei Darussalam. Journal of the Geological Society, 156(3), 633–650. doi: 10.1144/gsjgs.156.3.0633.

Wang ZF, Huang BJ. 2008. Dongfang 1–1 gas field in the mud diapir belt of the Yinggehai Basin, South China Sea. Marine and Petroleum Geology, 25(4–5), 445–455. doi: 10.1016/j.marpetgeo.2008.01.004.

Wang XJ, Hutchinson DR, Wu SG, Yang SX, Guo YQ. 2011. Elevated gas hydrate saturation within silt and silty clay sediments in the Shenhu area, South China Sea. Journal of Geophysical Research. Solid Earth, 116(B5), B05102. doi: 10.1029/2010jb007944.

Wang XJ, Collett TS, Lee MW, Yang SX, Guo YQ, Wu SG. 2014. Geological controls on the occurrence of gas hydrate from core, downhole log, and seismic data in the Shenhu area, South China Sea. Marine Geology, 357, 272–292. doi: 10.1016/j.margeo.2014.09.040.

Wang ZF, He JX, Xie XN. 2004. Heat flow action and its control on natural gas migration and accumulation in mud-fluid diapir areas in Yinggehai Basin. Earth Science, 29(2), 203–210 (in Chinese with English abstract).

Wang ZX. 2000. Is capillary power a driving force for the primary migration of oil and gas? Petroleum Geology and Experiment, 22(3),

195–200 (in Chinese with English abstract). doi: 10.11781/sysydz200003195.

Westbrook GK, Carson B, Musgrave RJ. 1994. 1. LEG 146 Introduction: Cascadia Margin[1]. In: Proceedings of the Ocean Drilling Program, Initial report, 146(Part 1). College Station, TX: Texas A&M University, 5–14. doi: 10.2973/odp.proc.ir.146-1.001.1994.

Whiticar MJ. 1999. Carbon and hydrogen isotope systematics of bacterial formation and oxidation of methane. Chemical Geology, 161(1–3), 291–314. doi: 10.1016/S0009-2541(99)00092-3.

Wiese K, Kvenvolden KA. 1993. Introduction to microbial and thermal methane. United States Geological Survey, Professional Paper, 1570.

Wu NY, Zhang HQ, Yang SX, Zhang GX, Liang JQ, Lu JA, Su X, Schultheiss P, Holland M, Zhu YH. 2011. Gas hydrate system of Shenhu area, northern South China Sea: Geochemical results. Journal of Geological Research, 2011(1), 370298. doi: 10.1155/2011/370298.

Xia Y, Yang JX, Zhang W, Wei W, Han WF, Xing LC, Xia JL. 2024. The different roles of fluid conduits for marine gas hydrate systems: A global review. International Geology Review, 66(4), 855–883. doi: 10.1080/00206814.2023.2214816.

Xie YH, Li XS, Fan CW, Tan JC, Liu K, Lu Y, Hu WY, Li H, Wu J. 2016. The axial channel provenance system and natural gas accumulation of the Upper Miocene Huangliu Formation in Qiongdongnan Basin, South China Sea. Petroleum Exploration and Development, 43(4), 570–578. doi: 10.1016/S1876-3804(16)30067-2.

Xie X, Li S, He H, Liu X. 2003. Seismic evidence for fluid migration pathways from an overpressured system in the South China Sea. Geofluids, 3(4), 245–253. doi: 10.1046/j.1468-8123.2003.00070.x.

Xie XN, Li ST, Hu XY, Dong WL, Zhang MQ. 1999. Conduit system and formation mechanism of heat fluids in diapiric belt of Yinggehai Basin, China. Science in China Series D: Earth Sciences, 42(6), 561–571. doi: 10.1007/BF02877783.

Xu WY, Ruppel C. 1999. Predicting the occurrence, distribution, and evolution of methane gas hydrate in porous marine sediments. Journal of Geophysical Research: Solid Earth, 104(B3), 5081–5095. doi: 10.1029/1998JB900092.

Yan CZ, Shi HS, Wang XJ, Li YP, Li J. 2020. The occurrence, saturation and distribution of gas hydrate identified from three dimensional seismic data in the Lw3 area: The Northern Slope of the South China Sea. Offshore Technology Conference Asia. November 2–6, 2020. Kuala Lumpur, Malaysia. OTC, D012S001R093. doi: 10.4043/30387-ms.

Yang JX, Davies RJ, Huuse M. 2013. Gas migration below gas hydrates controlled by mass transport complexes, offshore Mauritania. Marine and Petroleum Geology, 48, 366–378. doi: 10.1016/j.marpetgeo.2013.09.003.

Yang R, Su M, Qiao SH, Cong XR, Su Z, Liang JQ, Wu NY. 2015. Migration of methane associated with gas hydrates of the Shenhu Area, northern slope of South China Sea. Marine Geophysical Research, 36(2–3), 253–261. doi: 10.1007/s11001-015-9249-9.

Ye JL, Wei JG, Liang JQ, Lu JG, Lu HL, Zhang W. 2019. Complex gas hydrate system in a gas chimney, South China Sea. Marine and Petroleum Geology, 104, 29–39. doi: 10.1016/j.marpetgeo.2019.03.023.

Yoo DG, Kang NK, Bo YY, Kim GY, Ryu BJ, Lee K, Lee GH, Riedel M. 2013. Occurrence and seismic characteristics of gas hydrate in the Ulleung Basin, East Sea. Marine and Petroleum Geology, 47, 236–247. doi: 10.1016/j.marpetgeo.2013.07.001.

You KH, Summa L, Flemings P, Santra M, Fang Y. 2021. Three-dimensional free gas flow focuses basin-wide microbial methane to concentrated methane hydrate reservoirs in geological system. Journal of Geophysical Research: Solid Earth, 126(12), e2021JB022793. doi: 10.1029/2021JB022793.

Zhang W, Liang JQ, Wei JG, Lu JA, Su PB, Lin L, Huang W, Guo YQ, Deng W, Yang XL, Wan ZF. 2020. Geological and geophysical features of and controls on occurrence and accumulation of gas hydrates in the first offshore gas-hydrate production test region in the Shenhu area, Northern South China Sea. Marine and Petroleum Geology, 114, 104191. doi: 10.1016/j.marpetgeo.2019.104191.

Zhang YZ, Xu XD, Gan J, Yang XB, Zhu JT, Yang JH, He XH, Guo XX. 2019. Formation condition and accumulation of Pliocene strata–trapped gas field L18 in the deepwater area of the Qiongdongnan Basin. Haiyang Xuebao, 41(3), 121–133 (in Chinese with English abstract). doi: 10.3969/j.issn.0253-4193.2019.03.012.

Zhang ZJ, Wright CS. 2017. Quantitative interpretations and assessments of a fractured gas hydrate reservoir using three-dimensional seismic and LWD data in Kutei basin, East Kalimantan, offshore Indonesia. Marine and Petroleum Geology, 84, 257–273. doi: 10.1016/j.marpetgeo.2017.03.019.

Zhong SL, Zhang JF, Luo JS, Yuan YJ, Su PB. 2021. Geological characteristics of mud volcanoes and diapirs in the northern continental margin of the South China Sea: Implications for the mechanisms controlling the genesis of fluid leakage structures. Geofluids, (1), 5519264. doi: 10.1007/s12665-016-5894-9.

Zuo TN, Wang R, He YL, Shi WZ, Liang JQ, Xu LT, Du H, Deng Y, Xu XF. 2022. Natural gas migration pathways and their influence on gas hydrate enrichment in the Qiongdongnan Basin, South China Sea. Geofluids, (1), 1954931. doi: 10.1155/2022/1954931.